ANTARCTIC OFFSHORE LEADS AND POLYNYAS AND OCEANOGRAPHIC EFFECTS

H. Jay Zwally and J. C. Comiso

Laboratory for Oceans, Goddard Space Flight Center, Greenbelt, Maryland 20771

A. L. Gordon

Lamont-Doherty Geological Observatory of Columbia University, Palisades, New York 10964

Abstract. Extensive areas of open water are located within the Antarctic sea ice pack in a near-shore zone of several hundred kilometers, as well as the marginal ice zone near the sea ice edge. The time-series of satellite passive microwave observations during 1974 provides quantitative values of the area of open water in the coastal zone and details of the opening and closing of polynyas on daily time scales. Along the coast, numerous polynya areas are observed. Sixteen study areas located over the continental shelf are analyzed to provide time series of the maximum brightness temperature (T_B), minimum T_B, average T_B, standard deviation of T_B within each study area, and the derived area of open water. Examination of the synoptic pressure maps in the Ross Sea indicates that the intermittent formation of a polynya near the ice shelf front is strongly influenced by the synoptic winds. Other polynya areas appear to be located offshore of major outlet glaciers that are locations of enhanced katabatic winds. In all cases, the intermittent increases in open water during the polynya events are superimposed on a significant background of near-shore open water, which averages about 19% during the winter period from March 17 through November 11 (days 76-315). In some locations, more open water is observed during the winter period than in the summer days November 12 through March 16 (316-75). The principal heat source in the near-shore zone during the winter is deduced to be latent heat from ice production as ice divergence continually produces new areas of open water. The oceanic heat from cooling of the shelf water column by itself would maintain open water for a period less than 30 days. The resulting ice production within the latent-heat polynyas and leads significantly contributes to the sea ice cover, which is generally driven from the continental shelf toward the deep ocean. Estimates of the rate of ice production along with the observed values of open water area are used to calculate the resultant salinization of the Antarctic shelf waters, giving increases in shelf water salinity of many tenths of parts per thousand during the winter months. Although uncertainties remain regarding the amount of ice exported from the shelves and the shelf-slope exchange of water required to maintain steady state shelf water salinity, it is concluded that ice formation in leads and polynyas over the shelf is likely to be a primary factor in the production of saline shelf water and ultimately in bottom water formation.

Introduction

The Antarctic sea ice pack is known to contain substantial areas of open water during all seasons (e.g., Priestley [1913] (see Bromwich and Kurtz [1982]); Zwally and Gloersen [1977]; Bromwich and Kurtz [1982]; Carsey [1980]; and Zwally et al. [1983]). The size, distribution, and duration of the open water areas within the ice pack are highly variable as the sea ice grows, deforms, and melts in response to atmospheric, oceanic, and radiative forcings. Principal factors influencing the Antarctic sea ice dynamics are the absence of geographical constraints to the northern edge of the ice pack and the strong near-shore drainage winds from the ice sheet [Kurtz and Bromwich, 1983; Parish, 1982]. The wind-induced divergence of the sea ice substantially reduces the time-averaged sea ice concentrations, particularly in the near-shore (inner) and marginal (outer) zones of the ice pack. During much of the year, ice production is rapid in the open water and thin ice areas that are continually formed near the coast. Net divergence of the near-shore ice is generally accompanied by a northerly transport of ice, which contributes to the expansion of the ice edge during the growth season and provides ice for melting at the outer edge [Hibler and Ackley, 1983]. Following the period of maximum winter ice extent, for example, the near-shore zone is expected to be a region of net ice production, and the marginal zone a region of net ice dissipation.

The recent realization of the extensive distribution of open water within the ice pack

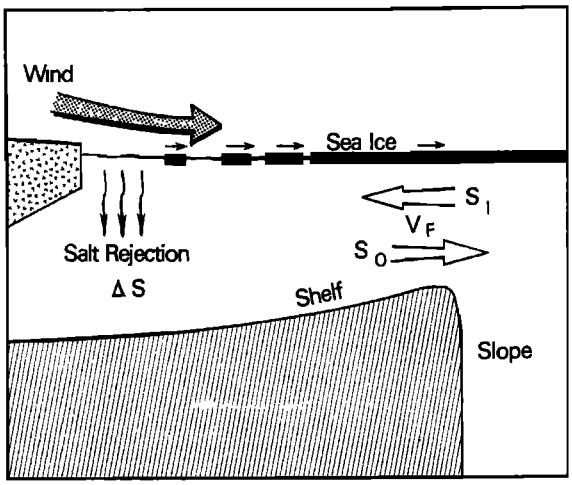

Fig. 1. Schematic diagram of ice production and salt rejection processes in near-shore regions of wind-induced divergence. V_F is the volume exchange rate between the inflow water with salinity S_I and outflow with salinity S_O. Other factors influencing the salt balance are discussed in the text.

is largely a result of year-round observations of the polar regions by passive microwave imagers flown on NASA research satellites over the last decade. The largest area of open water observed within the Antarctic sea ice pack is the Weddell polynya, which had approximately 2 x 10^5 km^2 of essentially ice-free ocean in some years (e.g. Zwally and Gloersen [1977]; Carsey [1980]; Martinson et al. [1981]; Parkinson [1983]). Except for the Weddell polynya, the sizes of the open water areas within the pack during winter are normally smaller than the 30-km resolution of the passive microwave imagers, and therefore the open water appears in the data as areas of reduced ice concentration.

In general, ice insulates the ocean, thereby sharply reducing the exchange of heat with the atmosphere. In the polynyas and leads created by ice deformation, the oceanic heat loss may be 10 to 100 times above that of the surrounding ice-covered surface (e.g., Maykut [1978]). The oceanic heat flux can be derived from two sources: (1) sensible heat of the sea water as it cools to the freezing point and (2) latent heat of fusion released during ice formation. In some situations during the winter period (when the heat flux is from the ocean to the atmosphere), open water may be maintained over a large polynya with little or no ice production, in which case the principal source of heat is therefore sensible heat from the ocean. In other situations where open water occurs in leads and small polynyas, the principal source of heat is latent heat from ice production. Therefore, open water features can be classified as primarily one of two types, either a sensible-heat or a latent-heat feature. These two types of features have significantly different effects on the ocean water. In the case of a sensible-heat feature, the open ocean continually cools to supply the heat flux to the atmosphere, as in the 1974-1976 Weddell polynyas during which the ocean cooled significantly to 2500 m depth [Gordon, 1982]. In the case of a latent-heat feature, where the sea ice is continually removed mechanically by the wind and the sensible heat from the ocean is inadequate to maintain an average open-water condition, new ice is continually created. The latter case leads to the production of large quantities of sea ice, which are subsequently carried to the surrounding waters.

Most of the polynyas described in the literature are probably of the latent-heat type, (e.g., the Saint Lawrence Island polynya in the Bering Sea, [Schumacher et al. 1983]; or the North Water polynya of Baffin Bay [Dey, 1980]). Within the southern ocean, sensible-heat polynyas are more likely in the deep-ocean region, where a large reservoir of relatively warm water (above 0°C) is found immediately below the shallow and weak permanent pycnocline. Upwelling and entrainment of this heat into the mixed layer is an important factor in the mixed-layer heat budget [Gordon, 1981; Gordon and Huber, 1984].

Over the continental shelf, the water column has an average temperature of -1.43°C (Table 1 from Carmack [1977]) and hence stores little heat above the freezing point. More sensible heat is available over the outer shelf where intrusions of slope water are more prevalent. Over the inner shelf, the water column is colder as the cold shelf water mass occupies a greater percentage of the depth and intrusions of slope water are significantly attenuated. Considering only the sensible-heat flux from open water to the atmosphere, a heat flux of 500 W/m^2 [Maykut, 1978; Schumacher et al., 1983], for example, would cool a 518 meter thick (mean depth [Carmack, 1977]) water column by 0.02°C/d. At this rate, the average shelf water column could sustain open water for only 23 days, not a full winter. Although an ocean circulation pattern that transfers all heat from the shelf waters into a restricted coastal region is conceivable, the sensible-heat flux required to sustain open water for the entire winter would cool the entire shelf volume to the freezing point, which is an unlikely condition since early summer data do not differ significantly from late summer data below the seasonal pycnocline. Therefore, the near-shore areas of open water are considered to be mostly latent-heat features, and thus, principal areas of ice production and salt rejection as shown schematically in Figure 1.

In this paper, the areas of open water in selected coastal regions and their temporal variability are described using passive microwave observations from the Nimbus 5 Electrically Scanning Microwave Radiometer (ESMR). The information on sea ice concentration from the microwave data set is much greater in spatial and temporal detail than other data in the sea ice zone, such as wind and temperature data. Although quantitative surface wind data are not available, examination of the time series of passive microwave data along with the synoptic sea level pressure maps in the Ross Sea, for example, indicates patterns of increases and decreases in sea ice concentration that are consistent with the surface wind fields deduced from the pressure maps. Quantitative values of the total area of open water derived from the passive microwave data for 16 coastal regions are used to estimate the resultant ice production and wintertime salinization of the shelf waters along the Antarctic coast.

Satellite Observations of Polynyas and Leads

Examples of the mean monthly sea ice concentrations derived from satellite microwave data are shown in Plate 1 using methods described below. Reduced ice concentrations in these time-averaged data are apparent in both summer and winter, particularly in the marginal ice zone and the near-shore zone. Open water (C < 14%) is observed where the Weddell polynya is forming in July 1974. The reduced ice concentrations near-shore during winter are most evident in locations of strong drainage winds such as the vicinity of the Ninnis and Mertz outlet glaciers around 148°E [Parish, 1982]. Sixteen study areas, which were chosen to enclose mostly shelf regions along the Antarctic coast, are outlined in Plate 1. The size and location of each area are given in Table 2. The locations of some of the study areas are based on the occurrence of significant offshore polynyas during the winter, and others are based on the absence of such polynyas. An interesting contrast occurs in some areas, such as the Shackleton area at 99°E and the Larsen at 59°W, where more open water is usually observed during winter than in summer (Plate 1). Variations of the open water areas on shorter time scales are described in the following analysis of daily and 3-day average brightness temperatures in the study areas.

Derived Sea Ice Concentration and Error Analysis

The observation and quantification of the amount of open water within the ice pack with passive microwave remote sensing is possible because of the large contrast between the emissivity of water and that of sea ice. The emissivities are approximately 0.44 for ice-free ocean and 0.92 for first-year sea ice at the ESMR wavelength of 1.55 cm. Thus, while the field-of-view of the satellite measurements is coarse (∿30x30 km), the relative areal coverage of open water and sea ice within a field of view can be derived.

In the simplest formulation, the observed microwave brightness temperature is a linear combination of the brightness temperatures of open water and sea ice, in proportion to the areal coverage of each within a field of view. Therefore, using the radiative transfer formulation and approximations described in Comiso and Zwally [1982] and Gloersen et al. [1974], the ice concentration (C) is

$$C(\%) = \frac{(T_B - T_O) \times 100}{\varepsilon_I T_{eff} - T_O} \qquad (1)$$

where T_B is the measured brightness temperature, T_O is the observed brightness temperature of ice-free ocean, and $\varepsilon_I T_{eff}$ is the observed brightness temperature of 100% ice cover. The ε_I is the microwave emissivity of sea ice, and T_{eff} is the temperature of the ice adjusted to incorporate the atmospheric effects as described in Comiso and Zwally [1982] and Zwally et al. [1983]. Similarly, T_O, which is approximately 135 K under average conditions, is equal to the microwave emissivity of seawater times its physical temperature, plus secondary terms due to atmospheric emissions. Inclusion of the atmospheric effects in T_O and T_{eff} as approximations retains the simple linear relationship between concentration and observed brightness temperature. A typical value of $\varepsilon_I T_{eff}$ is 235 K, which varies with either the emissivity or physical temperature of the ice.

The emissivity of sea ice in the southern ocean has been observed to have little variation, except during spring and summer when surface melt causes variations in emissivity from 0.85 to about 0.95 [Comiso et al., 1984]. Thus, since most of the data analyzed in this paper are from winter observations, a constant ice emissivity of 0.92 is assumed in the analysis. However, a significant localized effect occurs in the Bellingshausen-Amundsen Seas where a lower emissivity of the old ice surviving the summer melt lowers the derived ice concentration values for those areas by about 10%. Whereas the calculations of the ice concentrations in Plate 1 used climatological air surface temperatures to estimate T_{eff}, in this study the variations in the physical temperature of the ice from one study area to another and over the seasonal cycle are neglected by using an average value of 235 K for the maximum brightness temperature ($\varepsilon_I T_{eff}$) corresponding to 100% ice cover in equation (1).

TABLE 1. Error Analysis of Open Water Observations

	T_B^{MAX}	σ_M	T_B	δW_1 (%)	Area (Pixels)	Overlap (%)	δW_2(%)	δW (%)
Riiser-Larsen	233.6	6.4	215.2	1.1	10 x 5	8.6	2.6	2.8
Syowa	231.7	5.4	221.8	3.0	3 x 9	11.2	3.4	4.5
Amery	233.8	3.7	215.8	1.0	19 x 6	6.7	2.0	2.2
Prydz	228.2	3.9	208.1	5.3	7 x 6	5.6	1.7	5.6
Shackleton	234.0	4.9	207.1	1.0	9 x 7	4.3	1.3	1.6
Casey	234.6	4.4	217.7	0.3	9 x 7	4.9	1.5	1.5
Sabrina	236.6	4.6	223.6	-1.4	9 x 7	5.8	1.7	2.2
Adélie	228.9	3.7	209.6	4.9	7 x 8	3.9	1.2	5.0
George V	236.2	2.9	225.6	-1.1	9 x 8	3.9	1.2	1.6
Ross	230.9	2.2	212.8	2.2	9 x 18	3.7	1.0	2.4
Ruppert	226.7	3.2	203.1	6.2	3 x 18	11.0	3.3	7.0
Amundsen	234.1	4.0	211.8	0.7	13 x 10	2.7	0.8	1.1
Bellingshausen	236.8	5.1	220.9	-1.5	23 x 11	2.9	0.9	1.7
Larsen	235.5	5.1	214.8	-0.4	13 x 15	2.9	0.9	1.0
Weddell	237.9	2.7	229.0	-2.6	16 x 24	2.0	0.6	2.7
Halley	233.3	3.2	224.8	1.6	18 x 8	4.4	1.3	2.1

Using $\varepsilon_I = 0.92$, the value of 235 K for $\varepsilon_I T_{eff}$ implies an ice temperature of about 255 K and an air temperature of about 250 K.

The error in the derived ice concentration, or open water fraction (W = 100 - C), that is caused by variations in $\varepsilon_I T_{eff}$ is estimated with the following equation derived from equation (1)

$$\delta W(\%) = \frac{C\,\varepsilon_I\,T_{eff}}{\varepsilon_I T_{eff} - T_O} \simeq 0.007\ C\ \delta T_A \qquad (2)$$

Using $\varepsilon_I = 0.92$, $(\varepsilon_I T_{eff} - T_O) = 100$ K, and $T_{eff} \simeq T_I = 0.75\ T_A + 67.8$, where T_I is the temperature at the snow/ice interface and T_A is the surface air temperature [Zwally et al., 1983]. For example, if T_A were 255 K in an area where 10% open water is calculated using $\varepsilon_I T_{eff} = 235$ K, then δT_A is 5 K and the correct calculated value would be 13% open water using $\varepsilon_I T_{eff} = 238.2$ K. Therefore, the calculated amount of open water is too small in places that are physically warmer than 250 K and too large in places that are colder. Such temperature variations may be on the order of 5 to 10 K during the winter period (days 76 to 315) resulting in open water errors of 3 to 6%, but the average error over the winter is smaller. The time-series of the maximum observed brightness temperature (T_B^{MAX}), which corresponds to 100% ice cover in most study areas during the winter months, also indicate the possible errors due to using $\varepsilon_I T_{eff}$ fixed at 235 K. If the observed T_B^{MAX} is both representative of 100% ice cover and less than 235 K (note the 100% line in Figures 4, 5, and 9 through 23), then the calculated open water would be too large (or too small if T_B^{MAX} is greater than 235 K). To estimate the actual error due to using a fixed value of 235 K, it is assumed that T_B^{MAX} averaged over the midwinter (days 100 to 290) is representative of 100% ice cover and deviations (δT_B) of the average, $\langle T_B^{MAX} \rangle$, from 235 K cause errors. Actual deviations are expected to be due to variations in ice emissivity and temperature, which cause real errors, and to the intermittent occurrence of less than 100% ice cover throughout the study area, which does not cause real errors in the calculated open water. Therefore, the error estimates obtained here are probably upper limits. The standard deviation σ_M of T_B^{MAX} is an indication of both the short-term variability of the error during the season and departures from 100% ice cover in all pixels. The values of $\langle T_B^{MAX} \rangle$, the standard deviation σ_M, the midwinter average of the T_B averaged over each study area $\langle T_B \rangle$, and the estimate of the error $\langle \delta W_1 \rangle$ in the winter average open water are given in Table 1 using $\langle \delta W_1 \rangle \simeq C \delta T_B$, where

$$C \simeq T_B - 135 \text{ and } \delta T_B = \langle T_B^{MAX} \rangle - 235\ .$$

The values of $\langle \delta W_1 \rangle$ are mostly less than 5%.

Another source of error in the estimate of the open water in each study area is the overlap of some coastline ocean pixels on the ice shelf or ice sheet. The effect of the contaminated coastline pixels on the A_W value is limited by the ratio of coastline pixels to the total ocean pixels in each study area. The binary map used to differentiate land areas from ocean areas in the analysis of the data was constructed such that, if the center of the data element is over ocean, the data element is classified as ocean. Therefore,

the percentage contamination by ice shelf or ice sheet could range from 0 to about 50% in each coastline pixel. Assuming 25% contamination of the coastline pixels, the areal contamination ranges from about 2% to 11% of the total ocean pixel area as shown in Table 1. The actual effect on the calculated open water area also depends on the winter brightness temperatures inside the coastline compared to those outside the coastline. The T_B inside the coastline ranges from about 155 K on the Larsen Ice Shelf to about 185 K on the Ross Ice Shelf to about 215 K on parts of the East Antarctic ice sheet margin. For a T_B inside the coastline of 185 K, which falsely implies 50% open water, and a value of T_B = 215 K outside the coastline, the possible contamination error ranges from $\delta W_2 = 0.6\%$ to $\delta W_2 = 3.3\%$, corresponding to the areal contaminations of 2% and 11% respectively. Consequently, the estimated overall error $\langle \delta W \rangle$ in the calculated winter average open water area, including deviations of $\varepsilon_I T_{eff}$ from 235 K and the pixel contamination, is less than 5% (e.g., $\langle W \rangle = 19\% \pm 5\%$) in all areas except Prydz and Ruppert where it is 5.6% and 7.0%, respectively.

Another source of some uncertainity is the microwave emissivity of very thin ice under about 5 cm (new ice and dark nilas). While unconsolidated frazil ice, grease ice, and other new ice forms probably have microwave emissivities more like open water than first-year ice, thin ice of more than about 5-cm thickness (light nilas, gray ice, and gray-white ice) has an emissivity close to that of first-year ice. Therefore, some fraction of the areas of very thin ice under about 5 cm, including, in particular, areas of unconsolidated frazil ice and grease ice, may be included in the ESMR derived values of open water. Consequently, the area of totally ice-free water may be slightly less than the total area of open water indicated by the EMSR. However, this uncertainity is not significant for many purposes such as the estimation of heat fluxes and ice production because of the similarity of these quantities for both open water and very thin ice.

Both daily averages and 3-day averages of brightness temperatures are analyzed. The daily averages give better temporal resolution, while the 3-day averages give better spatial resolution because the three-day maps used only the center of the observation swath (1360 km versus 2500 km). Each map element is approximately 30 x 30 km, which along with other mapping characteristics and associated uncertainities are described in more detail in Zwally and Gloersen [1977], Zwally et al. [1983], and Comiso and Zwally [1984]. The daily average data thus enable the observation and identification of shorter-term polynyas and give better measure of their variability. However, most of the analyses presented in this paper use the 3-day average maps. When only one date is used to identify a 3-day average map, it is the first day of the 3-day period. Although the 3-day averages may include as many as about 35 observations in each map element distributed over the 3 days, in a few cases, some map elements may have only one or no observations due to the irregular data gaps.

Ross Sea Region

A good example of a recurrent polynya area is in the Ross Sea near the ice shelf front (Plate 2). Three sequences of color-coded images illustrate how the brightness temperature changes from one 3-day period to another. The first set of images (top two) shows the most pronounced change in brightness temperature, which is attributed to a substantial increase in the amount of open water during the 6-day interval from days 100-102 to 106-108. The overall ice condition recovered to a previous state after a few days, but a major change in ice cover occurred again 30 days later as shown in the second set, though not as pronounced as the first. Another significant change in ice cover occurred after another 30 days, but not as large as in either of the first two events. Sea ice concentration changes, similar in magnitude to the third event, occurred a few more times during the year.

The short-term nature of the changes in the Ross Sea suggests that the polynya events are principally driven by winds. Presumably, the reduced concentration is caused by divergence and ice transport from the area. Figure 2 shows transects of brightness temperatures along 179°E across the Ross Sea study area before, during, and after the April polynya event. Notable changes of the ice cover along the transect, including the ice edge, accompanied the change in ice cover in the vicinity of the shelf (e.g., see plot for Julian days 106 and 109). The increase in the sea ice concentration in the outer part of the pack and the slightly higher than normal rate of expansion of the ice edge during the polynya event are further indications of a synoptic-scale wind-driven effect, which is examined in more detail below. The T_B of the ice shelf and the continental ice sheet, in contrast, are relatively constant, and respond slowly to changes in the surface physical temperature (except under melting conditions). The size and location of some of the satellite data elements (pixels) representing the transects in Figure 2, are shown schematically in Figure 3. One pixel (43) is contaminated by contributions from the ice shelf, and the brightness temperature of this pixel did not decrease as much as those farther away from the boundary

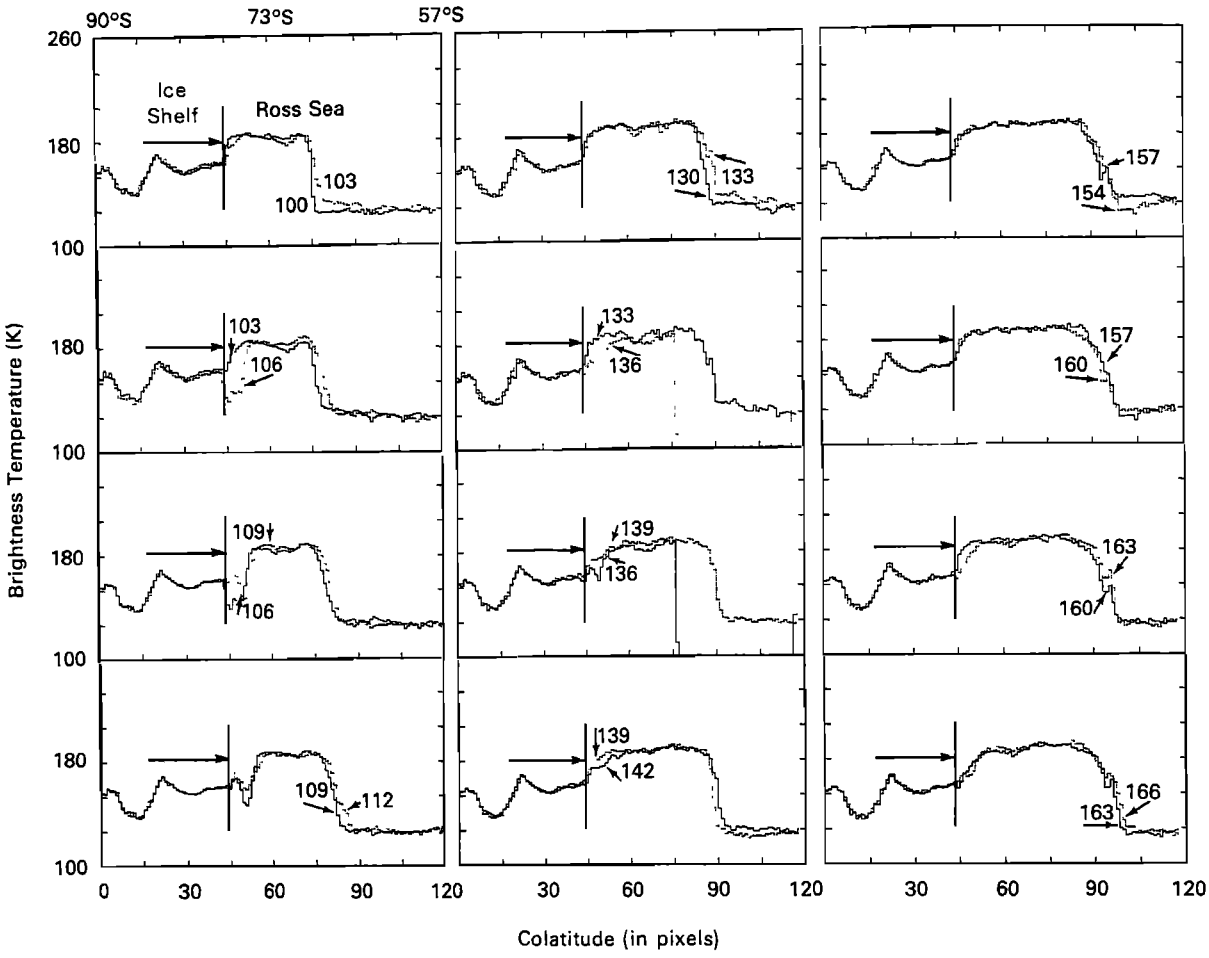

Fig. 2. Latitudinal transects of brightness temperatures along the Ross Ice Shelf and the Ross Sea during occurrences of the Ross Sea polynya.

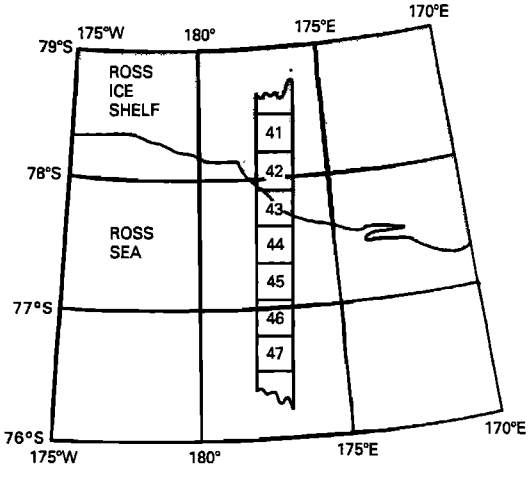

Fig. 3. Pixel (30 km x 30 km) locations along the transect crossing the ice shelf in Fig. 2.

during the occurrence of the polynya. The brightness temperature of the ice shelf in this pixel is substantially less sensitive to the atmospheric forcing.

Figures 4 and 5 show time-series of observed maximum and minimum brightness temperatures (T_B^{MAX} and T_B^{MIN}) in the Ross Sea study area using daily and 3-day averages of all good data in 1974. These time series are obtained by examining the T_B of each of the 123 map elements over the ocean part of the study area for each of the maps. Between January 1 and February 24 (Julian days 1 to 55), the maximum brightness temperature is about 185 K, indicating a maximum ice concentration within the study area of about 50% during summer. As previously noted, the series of T_B^{MAX} are useful for establishing the T_B of 100% ice cover, which is assumed to be found in at least one pixel in most of the maps during winter. From March 11 until November 21 (70-

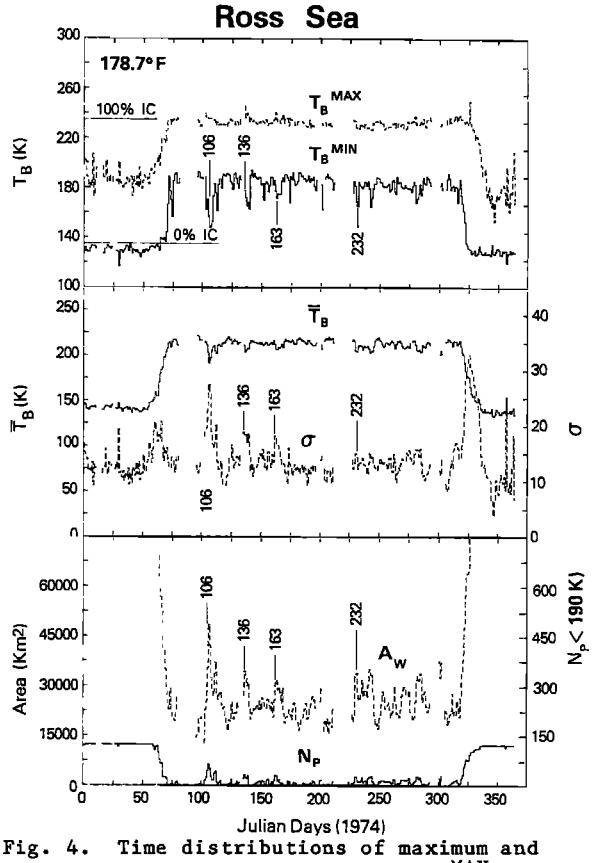

Fig. 4. Time distributions of maximum and minimum brightness temperatures (T_B^{MAX}), (T_B^{MIN}), mean ($\bar{T}_B$), standard deviations σ, number of pixels (N_p) with T_B < 190 K, and areal extents of open water (A_W) in the Ross Sea study area using 1-day average data.

325), the T_B^{MAX} is within a few degrees of 235 K. The small variation in the T_B^{MAX} during winter indicates that consolidated ice persisted in some parts of the area throughout this time.

The distribution of minimum T_B, on the other hand, shows a near constant value of 135 K in the summer, which is consistent with the presence of at least one ice-free data element in the study area. The T_B^{MIN} increases abruptly to about 180 K in the fall and remains approximately constant at this value throughout winter, except for the dips around April 16 (106), May 16 (136), and June 12 (163) (and a few smaller ones) consistent with the observed changes shown in Plate 2. In the 1-day average time series on April 17 (107), the T_B^{MIN} is 146 K, indicating the presence of about 89% open water in some part of the study area. In the 3-day average time series, the T_B^{MIN} is 156 K on April 16-18 (106-108), corresponding to 79% open water in at least one of the time-averaged map elements. The lower value of T_B^{MIN} on the one-day average for day 107, compared to the three-day average for 106-108, indicates that the nearly ice-free ocean (89% open water) occurred for only a brief time at the height of this event. Such intermittent formation of open water reduces the average ice-concentration in the coastal regions as shown, for example, in the monthly average in Plate 1.

The variability of the ice cover is quantified by the standard deviation (σ) of the T_B within the study area as plotted in Figures 4 and 5. The average brightness temperature ($\bar{T}_B$) distribution is very similar to that of T_B^{MIN}, but the dips observed in the average T_B series are not as large as in the minima. During the summer, when the whole study area is occupied by a uniform mixture of water and a low concentration of ice floes, and in late winter when the area is predominantly consolidated ice, the standard deviation is smallest and least variable in its magnitude. The standard deviation increases in early fall around March 1 (60), when the study area is no

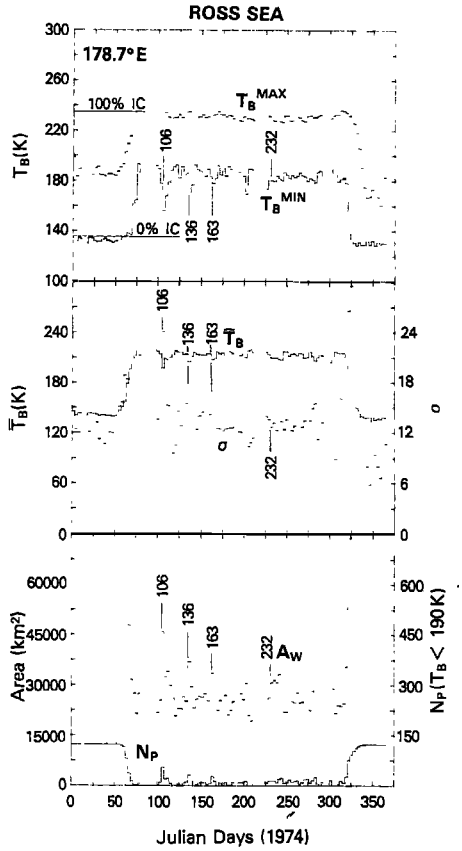

Fig. 5. Time distributions of maximum, minimum, and mean brightness temperatures, standard deviations, number of pixels < 190 K, and areal extents of open water in the Ross Sea study area using 3-day average data.

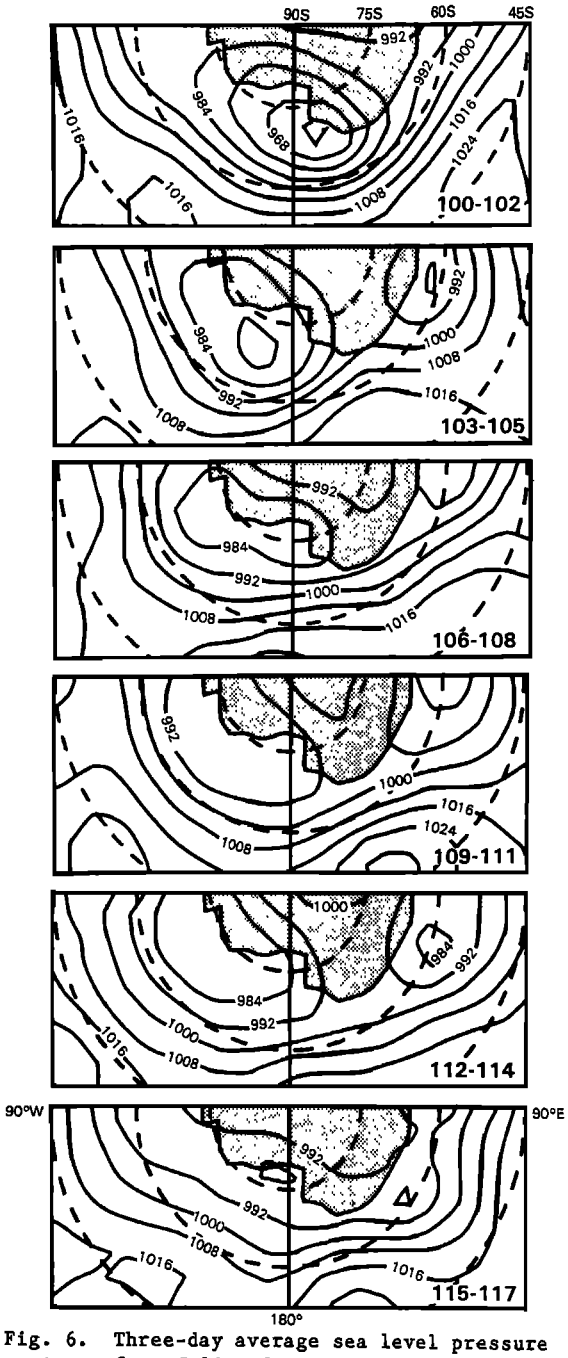

Fig. 6. Three-day average sea level pressure contours from Julian date 100 to 117, 1974.

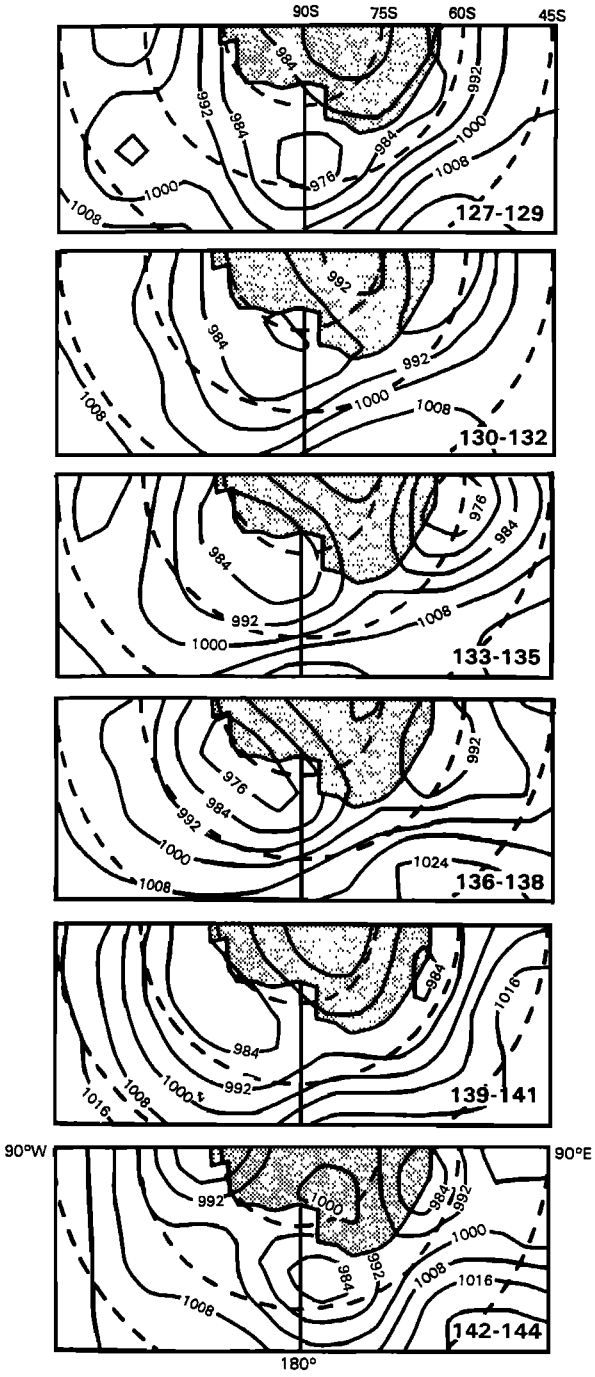

Fig. 7. Three-day average sea level pressure contours from Julian date 127 to 144, 1974.

longer uniform because of the introduction of newly frozen ice, and in the spring around November 21 (325) when substantial melting and breakup occur within the pack. The standard deviation also increases during the polynya events, indicating enhanced ice dynamics.

The areal extent and persistence of the polynya events, as well as the background of nonresolved open leads and polynyas, is quantified by applying equation (1) to each pixel to calculate the area of open water. The results for the Ross Ice Shelf study area are shown in Figures 4 and 5. The peak value of the total area of open water (A_W) in the study

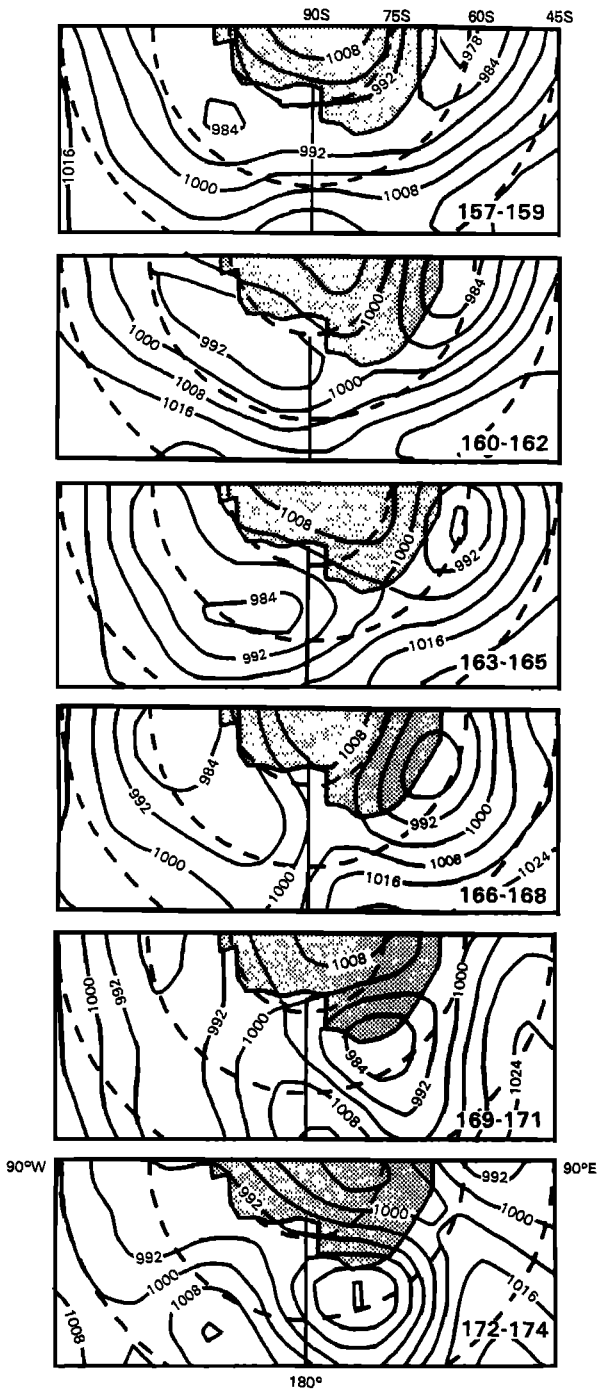

Fig. 8. Three-day average sea level pressure contours from Julian date 157 to 174, 1974.

area is 48,500 km^2 in the 1-day average for April 17 (107) of the first polynya event and 45,870 km^2 in the 3-day average for April 16-18 (106-108). Thus, the peak values of open water are larger in the 1 day than the 3-day averages, and the minima between the polynya events also tend to be smaller. However, the averages over 3 or more days are the same in each data set, and the average amount of open water during the winter in the Ross Sea study area is approximately constant at 27,000 km^2. The envelope of the maximum open water in the polynya events decreases to a minimum around mid-July (day 200) when the data indicate that the ice pack is most stable.

The role of synoptic wind in the formation of the Ross Ice Shelf polynya is illustrated by a qualitative analysis of 3-day average pressure contours in Figures 6, 7, and 8 before, during, and after the three polynya events shown in Plate 2. The data were interpolated from the Australian data set that had been prepared for studies of the influence of the wind fields on the position and variability of the ice edge during several seasons of growth and decay [Cavalieri and Parkinson, 1981; Parkinson and Cavalieri, 1982].

The cyclone system, centered near 170°E on days 100-102, migrated to the east to near 150°W on days 103-105 and further to the east to near 135°E on days 109-111. The cyclone position is also shown by the harmonic analysis [Cavalieri and Parkinson, 1981] of the pressure between 60° and 70°S, which is the nominal position of the circumpolar trough in the atmosphere. The increase in open water during the polynya event peaking on days 106-108 coincides with the shift of winds from easterly to southeasterly in front of the ice shelf as indicated by the pressure maps. Since the direction of ice drift is approximately in the direction of the surface winds, the open water during the polynya event is presumably caused by an enhanced northward ice drift. The more rapid increase of the open water during the event compared to the decay is also consistent with the rapid eastward movement of the strong cyclonic system, which was followed by a slower decay of the cyclone in its eastward position over the Amundsen Sea. Similar migrations of weaker cyclonic systems coincide with the weaker polynya events on days 130-132 and 160-162 as shown in Figures 7 and 8.

Changes in the T_B distribution over the ice pack indicate convergence or divergence in response to the wind field. For example, increased T_B indicates a more compact ice pack due to ice convergence or freezing. A small increase in the maximum T_B during the polynya events is evident in the T_B series (Figures 4 and 5) and on the T_B maps (Plate 2) in the eastern portion of the study area. During event 106-108, in particular, the ice in the southeastern part of the Ross Sea appears to be converging in response to the northerly winds at the same time the southeasterly winds in the southwestern part of the Ross Sea are producing open water. Similar changes in the ice edge are also related to the surface

winds. For example, the marked expansion of the ice edge by about 250 km around 170°E from days 100-102 to days 106-108 coincides with strong northerly winds that enhance ice growth and northward ice advection.

Other Study Regions

The set of parameters

$$T_B^{MAX},\ T_B^{MIN},\ \bar{T}_B,\ \sigma,\ A_W,\ \text{and}\ N_P$$

in Figures 9 to 23 describe various features of the open water areas and the polynya events for the other 15 study areas. As previously noted, T_B^{MAX} approximately indicates the maximum ice concentration in any of the 30 x 30 km pixels in the study area, and T_B^{MIN} usually indicates the minimum ice concentration. However, T_B^{MIN} is not always an accurate measure of the minimum ice concentration, because the pixel in which T_B^{MIN} is observed may be located partially (or completely due to coastline inaccuracies) over continental ice, which has brightness temperatures in the range of 150 K to 250 K. Because the T_B inside the coastline varies slowly during winter in response to the changing physical temperature, short-term decreases in T_B^{MIN} during winter do indicate polynya events nevertheless. Such events may be located in only one pixel, however, whereas increases in A_W represent the total change in open-water coverage over the entire study area. For example, a large drop in T_B^{MIN} with a small rise in A_W indicates a localized event within the study area. Changes in N_p (the number of pixels with T_B < 190 K) are also an indication of the spatial extent of an event. Changes in T_B and A_W are inversely proportional to each other, and σ is an indication of the variation of the open water around a mean value over the study area. As discussed below, substantial differences in the seasonal variations in these parameters from one study area to another are observed. In some areas, the approximate length of the ice growth season can be deduced from T_B^{MIN}, but in several areas T_B^{MIN} and the amount of sea ice cover are greater in summer than in winter.

The summer ice conditions are significantly different in the various study areas as can be seen in Plate 1, Figure 5, and Figures 9-23. In the George V and Larsen areas, the minimum T_B do not indicate ice-free water in any pixel at any time during the year. In the Syowa, Shackleton, Sabrina, and Ruppert areas, the minimum T_B indicates low concentrations in at least one pixel, but not totally ice-free water even in the summer. The other 10 areas all show some ice-free pixels during summer.

The maximum T_B is lowest in late summer indicating the absence of 100% ice cover at the end of the melt season in all study areas except the Weddell. Some of the maximum T_B distributions tend to increase slightly in value from fall to midwinter, indicating a higher probability of finding highly consolidated ice later in the growth season. Slight increases in maximum T_B above 235 K during spring are due to the known increase in the emissivity of the surface during the onset of melt [e.g., Zwally and Gloersen, 1977; Comiso, 1983].

The variability in the ice cover over each of the study areas, as indicated by σ, is in most cases greatest during the spring and summer breakup, with a tendency to decrease to a low value in late summer followed by an increase as the ice pack expands in early fall. There is also a tendency in many areas for σ to decrease to a minimum in midwinter indicating a more uniform ice cover, as for example in the Casey and Halley areas (Figures 14 and 23). The most notable exception to this pattern is exhibited in the Larsen area where the is largest in midwinter. In some areas such as Amery, Prydz, Casey, Sabrina, George V, and Ross, the has frequent abrupt changes due to dynamic activity of the ice pack. Also, in some of these cases, the abrupt changes in σ have associated abrupt changes in A_W as in the Prydz, George V, and Ross, but in others the concurrent changes in A_W are less marked due to differences in the way the open water is distributed across the study areas.

The most significant parameter is A_W, which is also most useful for identifying polynya events during which the area of open water increases markedly. In most areas, A_W is largest in late summer and decreases to a minimum in midwinter to late winter when the ice pack is expected to be mostly consolidated in the coastal regions. The most notable exception to this pattern of seasonal variation in A_W occurs in the Larsen area where the maximum A_W occurs in fall and the minimum A_W in summer. The A_W in the Larsen area is actually large throughout the winter, decreasing steadily from its maximum to minimum over a 9-month interval. The time variation of A_W in the Shackleton area is also similar to that in the Larsen.

In general, the production of open water in coastal areas is dependent on the atmospheric and oceanic forcings and the strength of the ice pack. The increase in thickness and consolidation of the ice pack in the coastal regions during the growth season may be a principal factor in the general decline in the open water exhibited in most areas during the winter months. As previously discussed, the production of open water in coastal regions during winter months is mainly wind driven. Therefore, the greater amounts of open water in the Larsen and Shackleton areas during winter than summer indicate a significantly stronger wind forcing of the ice pack in winter, whereas the wind and ocean current forc-

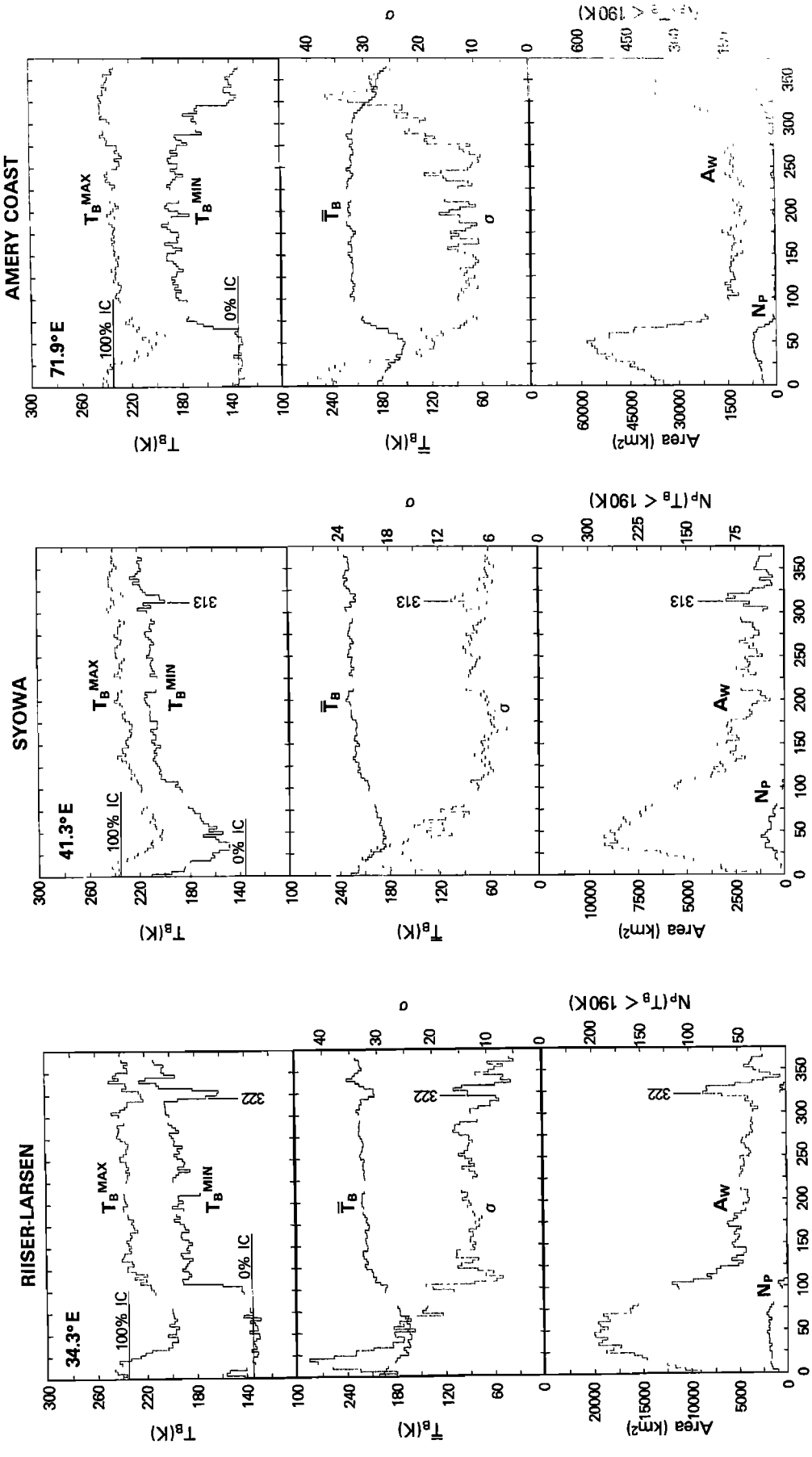

Fig. 9. Time distributions of maximum, minimum, and mean brightness temperatures, standard deviations, number of pixels < 190 K, and areal extents of open water in the Riiser-Larsen Ice Shelf study area using 3-day average data.

Fig. 10. Time distributions of maximum, minimum, and mean brightness temperatures, standard deviations, number of pixels < 190 K, and areal extents of open water near the Syowa study area using 3-day average data.

Fig. 11. Time distributions of maximum, minimum, and mean brightness temperatures, standard deviations, number of pixels < 190 K, and areal extents of open water in the Amery Ice Shelf study area using 3-day average data.

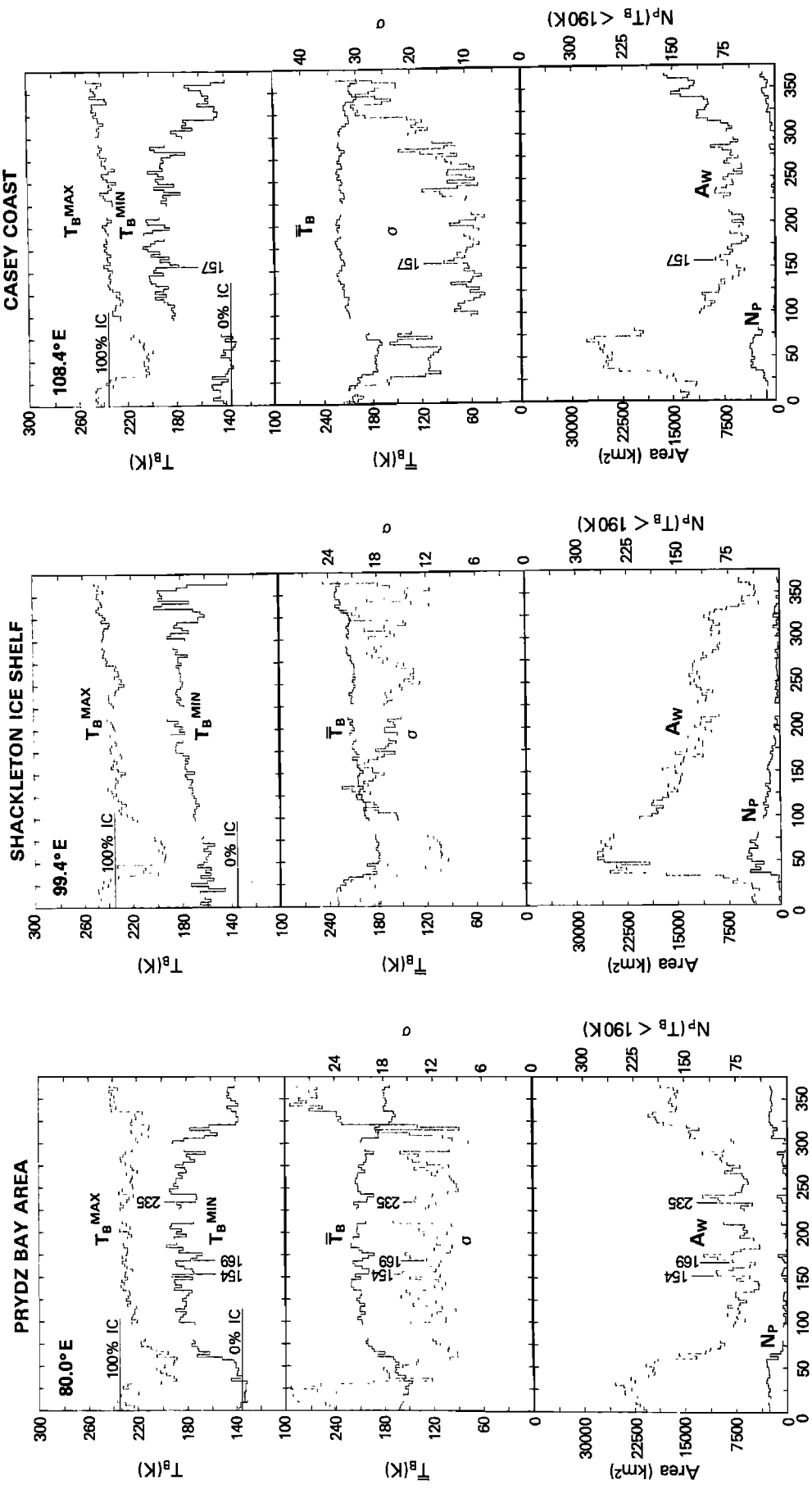

Fig. 12. Time distributions of maximum, minimum, and mean brightness temperatures, standard deviations, number of pixels < 190 K, and areal extents of open water in the Prydz Bay study area using 3-day average data.

Fig. 13. Time distributions of maximum, minimum, and mean brightness temperatures, standard deviations, number of pixels < 190 K, and areal extents of open water in the Shackleton Ice Shelf study area using 3-day average data.

Fig. 14. Time distributions of maximum, minimum, and mean brightness temperatures, standard deviations, number of pixels < 190, and areal extents of open water in the Casey study area using 3-day average data.

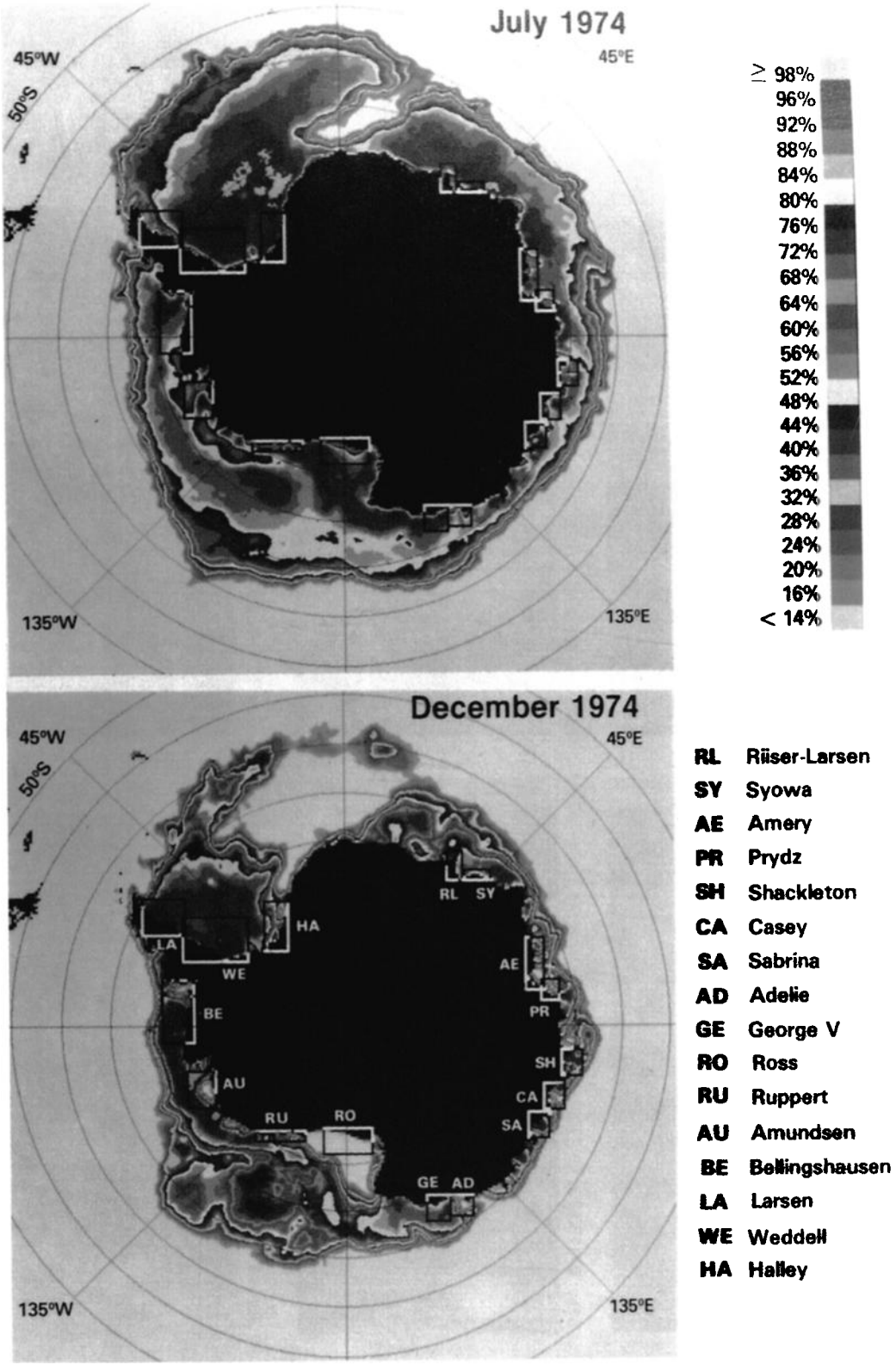

Plate 1. Sea ice concentration map inferred from Nimbus 5 ESMR for July 1974 and December 1974 (from Zwally et al. [1983] with study areas outlined).

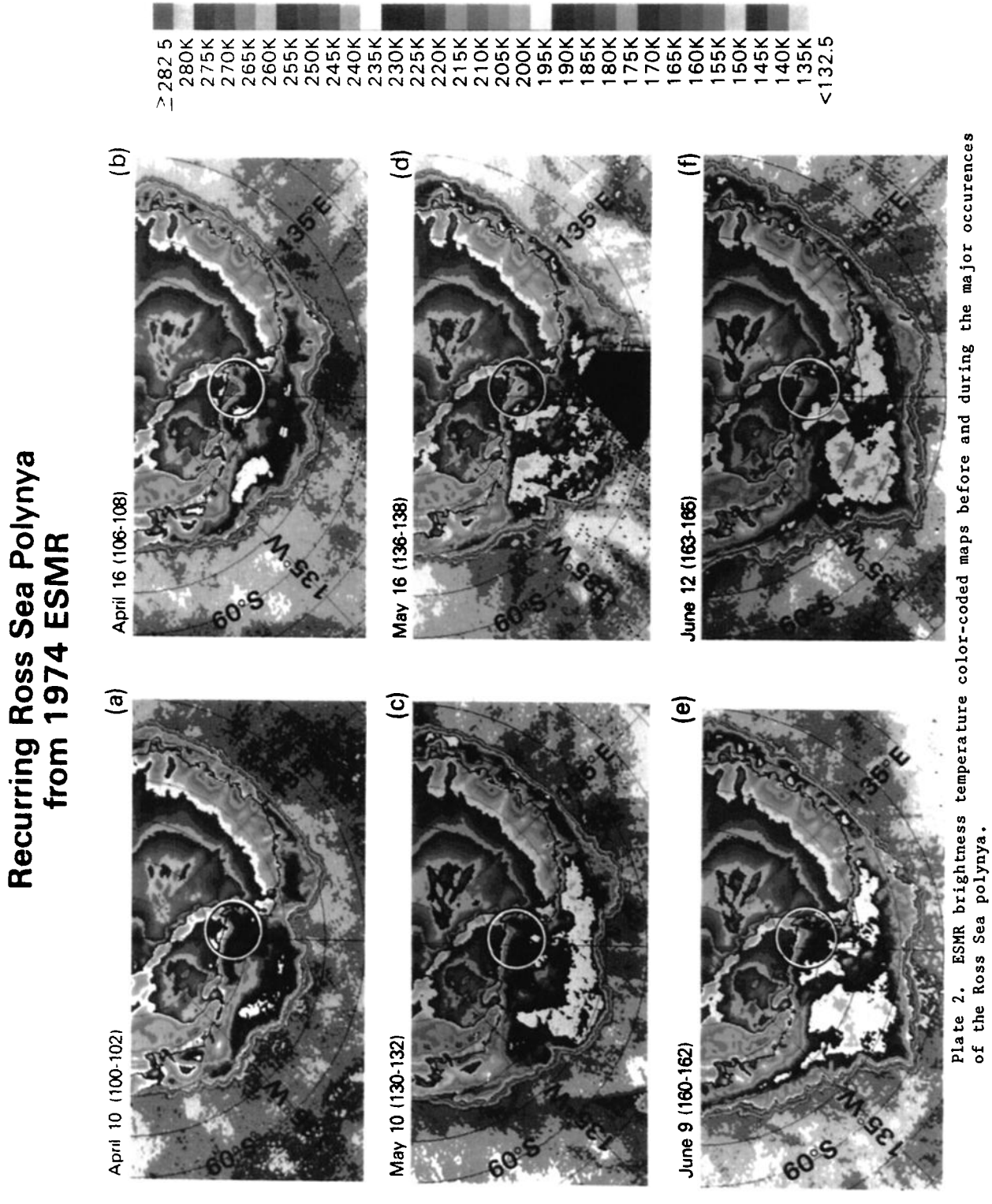

Plate 2. ESMR brightness temperature color-coded maps before and during the major occurences of the Ross Sea polynya.

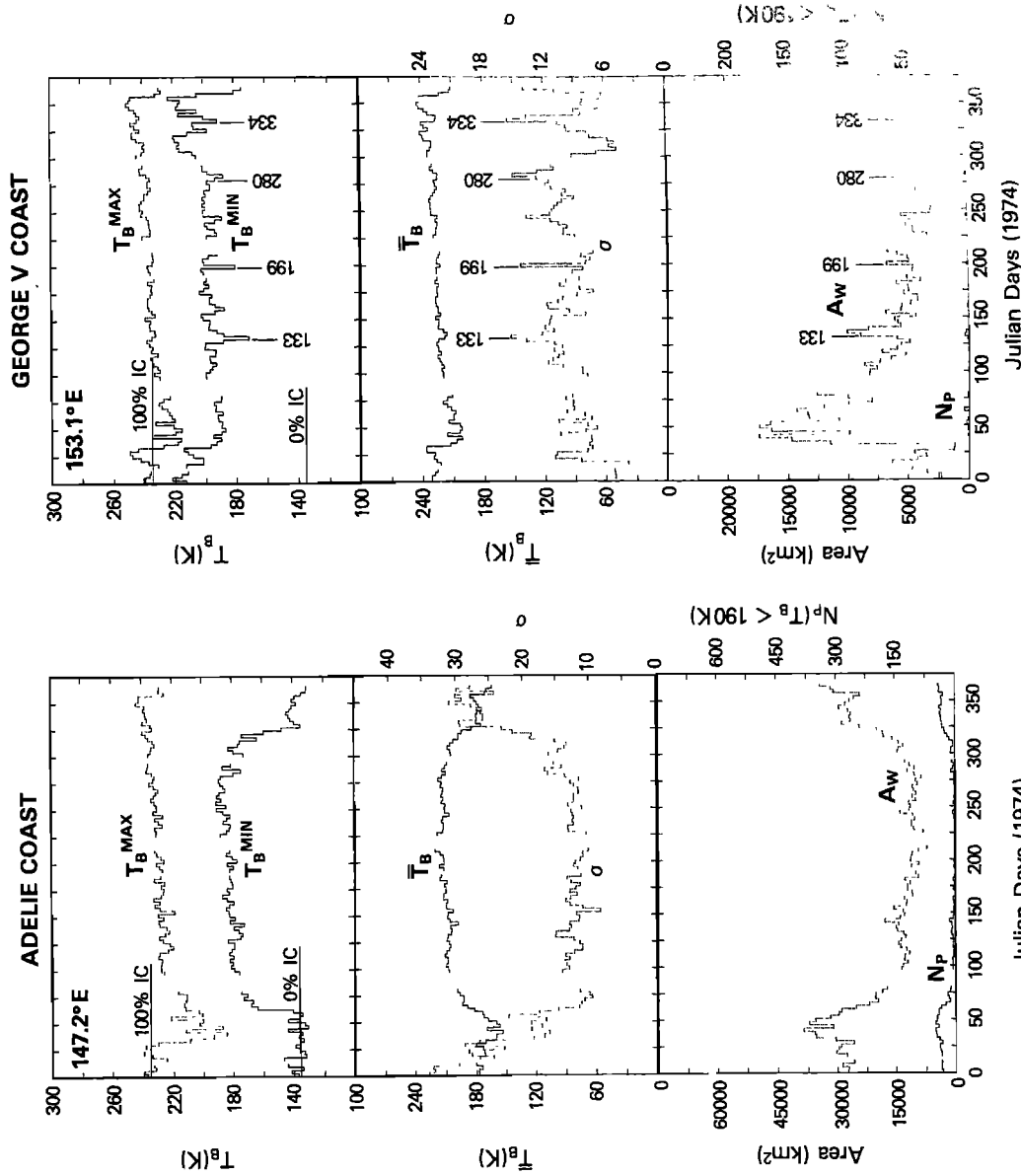

Fig. 15. Time distributions of maximum, minimum, and mean brightness temperatures, standard deviations, number of pixels < 190K, and areal extents of open water in the Sabrina Coast study area using 3-day average data.

Fig. 16. Time distributions of maximum, minimum, and mean brightness temperatures, standard deviations, number of pixels, and areal extents of open water in the Adélie Coast study area using 3-day average data.

Fig. 17. Time distributions of maximum, minimum, and mean brightness temperatures, standard deviations, number of pixels < 190 K, and areal extents of open water in the George V Coast study area using 3-day average data.

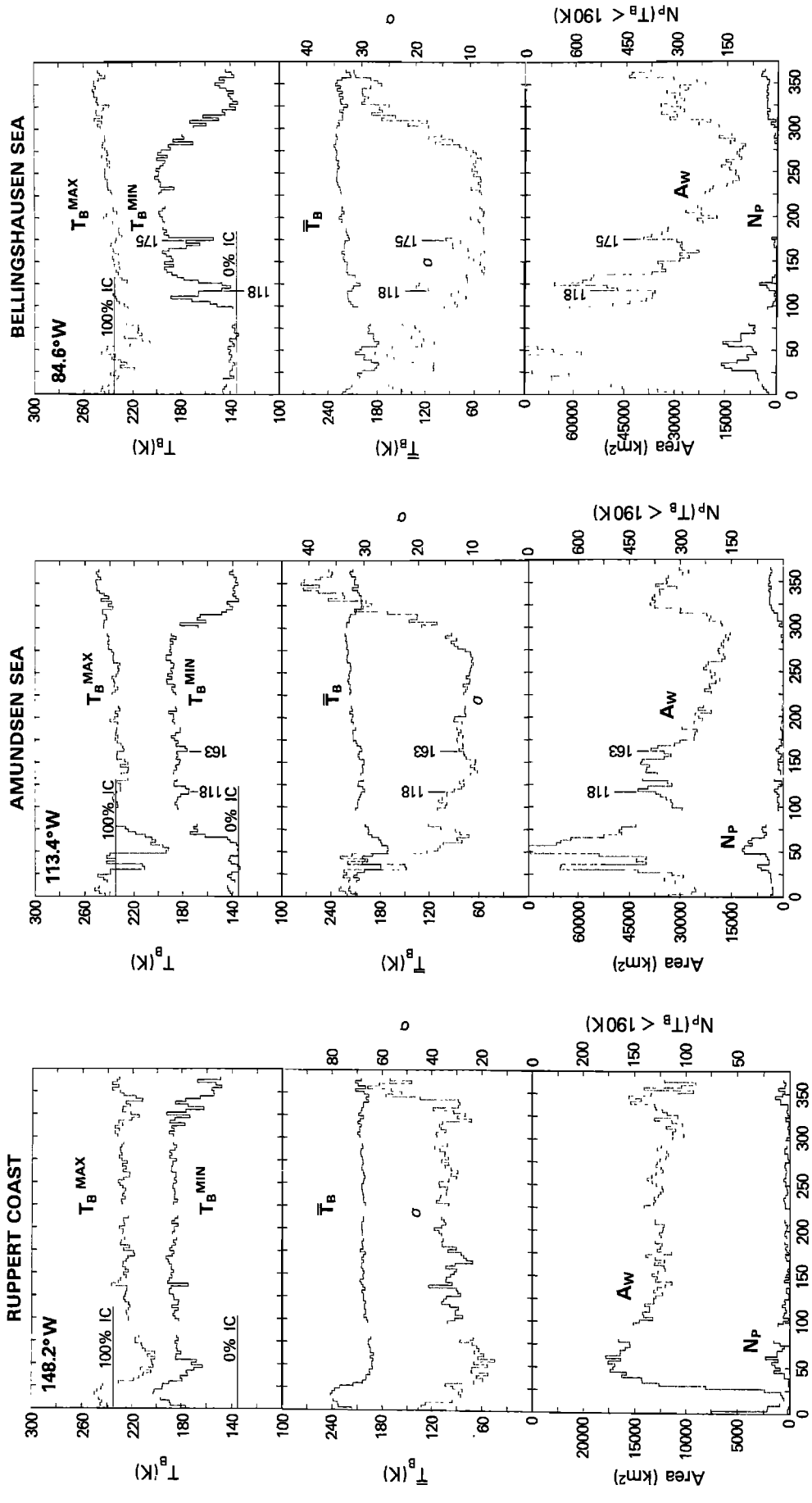

Fig. 18. Time distributions of maximum, minimum, and mean brightness temperatures, standard deviations, number of pixels < 190 K, and areal extents of open water in the Ruppert Coast study area using 3-day average data.

Fig. 19. Time distributions of maximum, minimum, and mean brightness temperatures, standard deviations, number of pixels < 190 K, and areal extents of open water in the Amundsen Sea study area using 3-day average data.

Fig. 20. Time distributions of maximum, minimum, and mean brightness temperatures, standard deviations, number of pixels < 190 K, and areal extents of open water in the Bellingshausen Sea study area using 3-day average data.

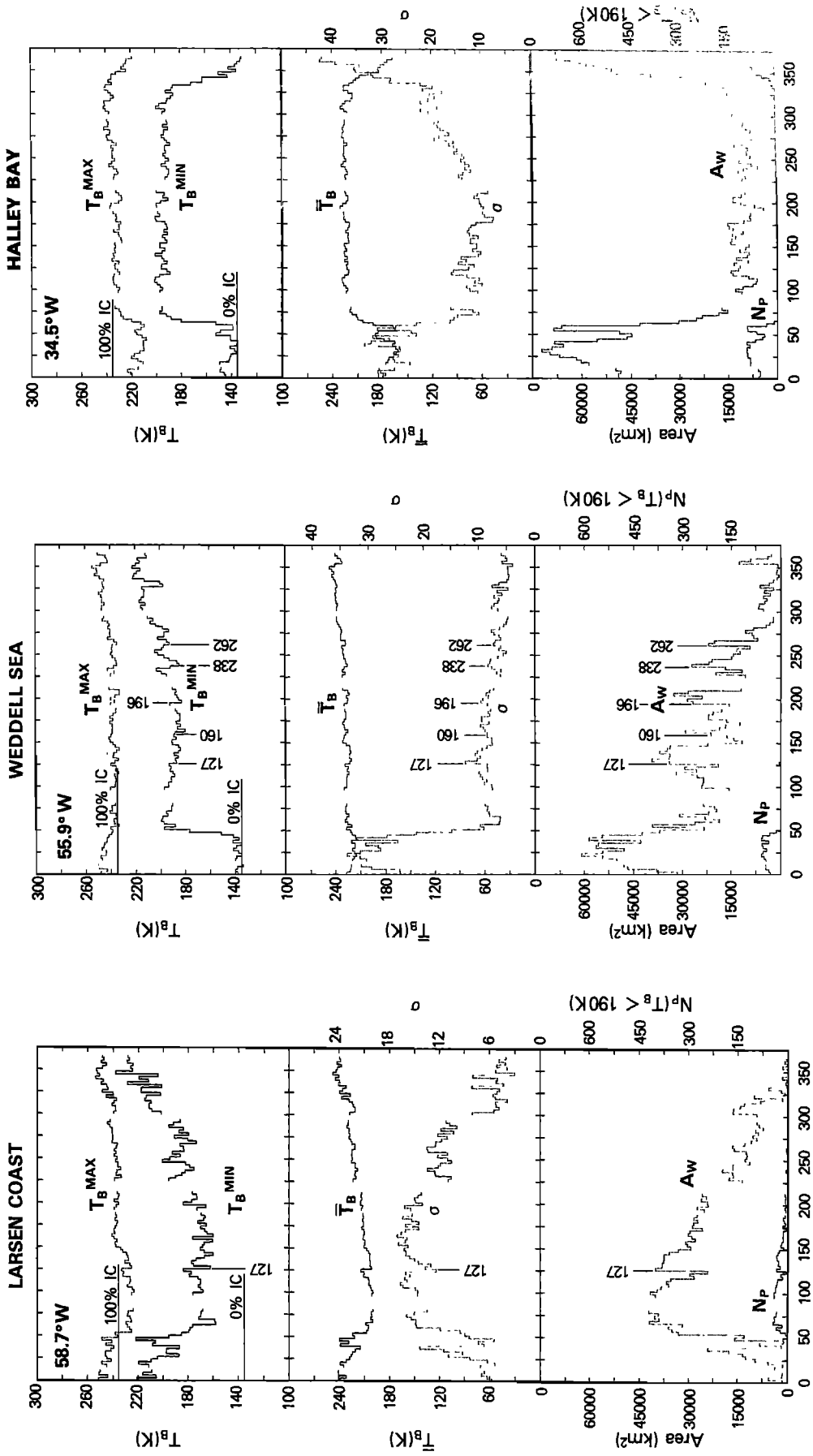

Fig. 21. Time distributions of maximum, minimum, and mean brightness temperatures, standard deviations, number of pixels < 190 K, and areal extents of open water in the Larsen Ice Shelf study area using 3-day average data.

Fig. 22. Time distributions of maximum, minimum, and mean brightness temperatures, standard deviations, number of pixels < 190 K, and areal extents of open water in the Weddell Sea study area using 3-day average data.

Fig. 23. Time distributions of maximum, minimum, and mean brightness temperatures, standard deviations, number of pixels < 190 K, and areal extents of open water in the Halley Bay study area using 3-day average data.

ing in these two areas in summer are apparently favorable for maintaining the observed consolidated ice cover.

Some of the more notable polynya events, in addition to those previously discussed in the Ross area are: in the Riiser-Larsen beginning around day 322; Syowa around day 313; Prydz around days 154, 169, and 235; Casey around day 157; Sabrina around days 265 and 340; George V around days 133, 199, 280, and 334; Amundsen around days 118 and 163; Larsen near day 127; and the Weddell around days 127, 160, 196, 238, and 262. The duration of these events is typically about 9-18 days, which may be associated with changes in the synoptic wind forcing as discussed for the Ross area. However, examination of the pressure maps in the Weddell Sea region did not show similar relations with the ice cover changes in the Larsen and Weddell, possibly because of the barrier influence of the Antarctic Peninsula [Parish, 1983] or inadequacies of the pressure maps. During the event in the Weddell area commencing on day 127, the large (50 x 90 km) tabular iceberg, which was grounded in front of the Ronne Ice Shelf near 77°S and 50°W, became ungrounded and moved 100 km northward to its position in Plate 1 [Zwally and Gloersen, 1977]. During these events in the Weddell Sea, the lowest sea ice concentrations are observed within about 100 km along the ice shelf front. The movement of the iceberg and the reduced ice concentrations are indicative of strong southerly winds. In the Bellingshausen, the increased open water after days 118 and 175 is caused by a retreat of the ice edge into the study area.

The Adélie and the George V areas show some interesting contrasts. The Adélie is located offshore of the Ninnis and Mertz glaciers and has tongues of reduced ice concentration extending over 100 km offshore in winter (Plate 1). The open water is greater in the Adélie area than the George V, but is less variable as shown by changes in both σ and A_W in Figures 16 and 17. The open water offshore from the glaciers is persistent and extends farther offshore than the typical distance of several tens of kilometers over which katabatic winds are usually substantially diminished [e.g., Bromwich and Kurtz, 1984]. Therefore, the variations observed in the coastal open water in these areas suggest that the Adélie is a location of persistent winds at substantial distances offshore from the glaciers, and the George V is a location of more localized and intermittent wind forcing.

In the following sections, the observed A_W is used to estimate the ice production and salinization of the shelf waters. As noted, in some areas the ice-growth season in the coastal regions can be inferred from the temporal changes in T_B^{MIN}, T_B^{MAX}, and the other parameters, but not in all areas as for examples, George V, Larsen, and Ruppert. Consequently, the growth (or winter) season is estimated for all areas to be from days 76 through 315 inclusive (240 days) and the melt (or summer) to be days 316 through 75 (115 days). The frequency distributions of the ratio of A_W to the total ocean area (A_T) for the winter and summer periods in each of the study areas are shown in Figures 24 and 25. All areas have more open water in summer than in winter except the Larsen and Shackleton. The average open water fraction in winter ($\langle A_W \rangle / A_T$) ranges from about 7% in the Weddell to about 25% in the Prydz, Shackleton, Adélie, Amundsen, Ross, and Ruppert (Table 2). These values of open water for the coastal zone are significantly larger than the values in the central part of the ice pack, but are close to the average over the entire pack including the marginal zone where the ice is most divergent. Figures 24 and 25 also show how variable the open water is during the summer and winter periods. In some places, like Amery and Halley, the open water area in winter does not vary much, whereas, in some other areas like Amundsen and Larsen, A_W changes substantially from early winter to late winter. The width of the distributions is also affected by the occurrences of polynyas. To quantify this variability of A_W/A_T, a Gaussian function with a linear background was fitted to each winter distribution by methods of least squares, and the standard deviation (σ_A) of the Gaussian for each study area is given in Table 2.

Oceanic Effect of Offshore Leads and Polynyas

In regions of sea ice and open water such as the Antarctic shelf that do not have significant heat storage in the water column, heat flux into the atmosphere will be derived primarily from the latent heat of fusion. For this situation, estimates of heat flux and daily ice production have been made by Schumacher et al. [1983] for the Saint Lawrence Island polynya in the Bering Sea, based upon changes of water column salinity. For the Antarctic shelf, estimates have been made by Cavalieri and Martin [this volume] based on meteorological data from nearby coastal stations. Schumacher et al. (1983] determine a heat flux of 535 W m^{-2} with an ice production of 0.17 m/d. Cavalieri and Martin [this volume] find an average 90-day ice production of 9 m (their Table 4), which is equivalent to 0.10 m/d, and their average heat flux is 300 W m^{-2}.

The brine rejection associated with ice production within the open water areas increases the water column salinity over what is expected from ice growth through bottom accretion alone. The salinity increase due solely

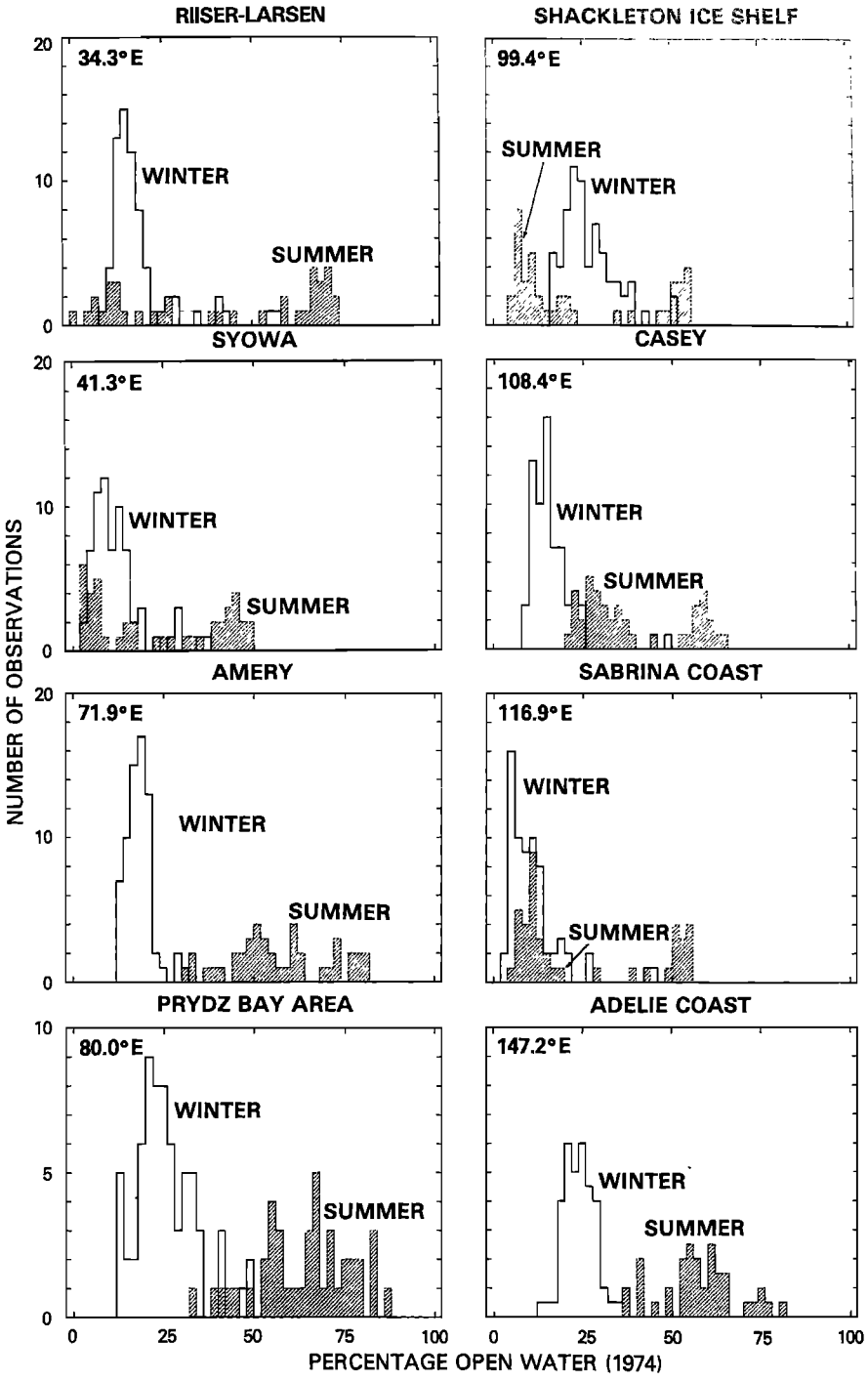

Fig. 24. Frequency distributions of the ratio of open water area to total area in each of the study regions from 34°E to 147.5°E.

to new ice growth in open water areas is estimated for each study area by

$$\Delta S = \frac{s\ T\ A\ R_i}{0.1\ h} \qquad (3)$$

where ΔS is the salinization of the total volume of shelf water within the study region, scaled by the 0.1 to units of °/₀₀, s is the salt rejection in g cm^{-2} for each meter of sea ice formation (a value of 2.5 g cm^{-2} is used,

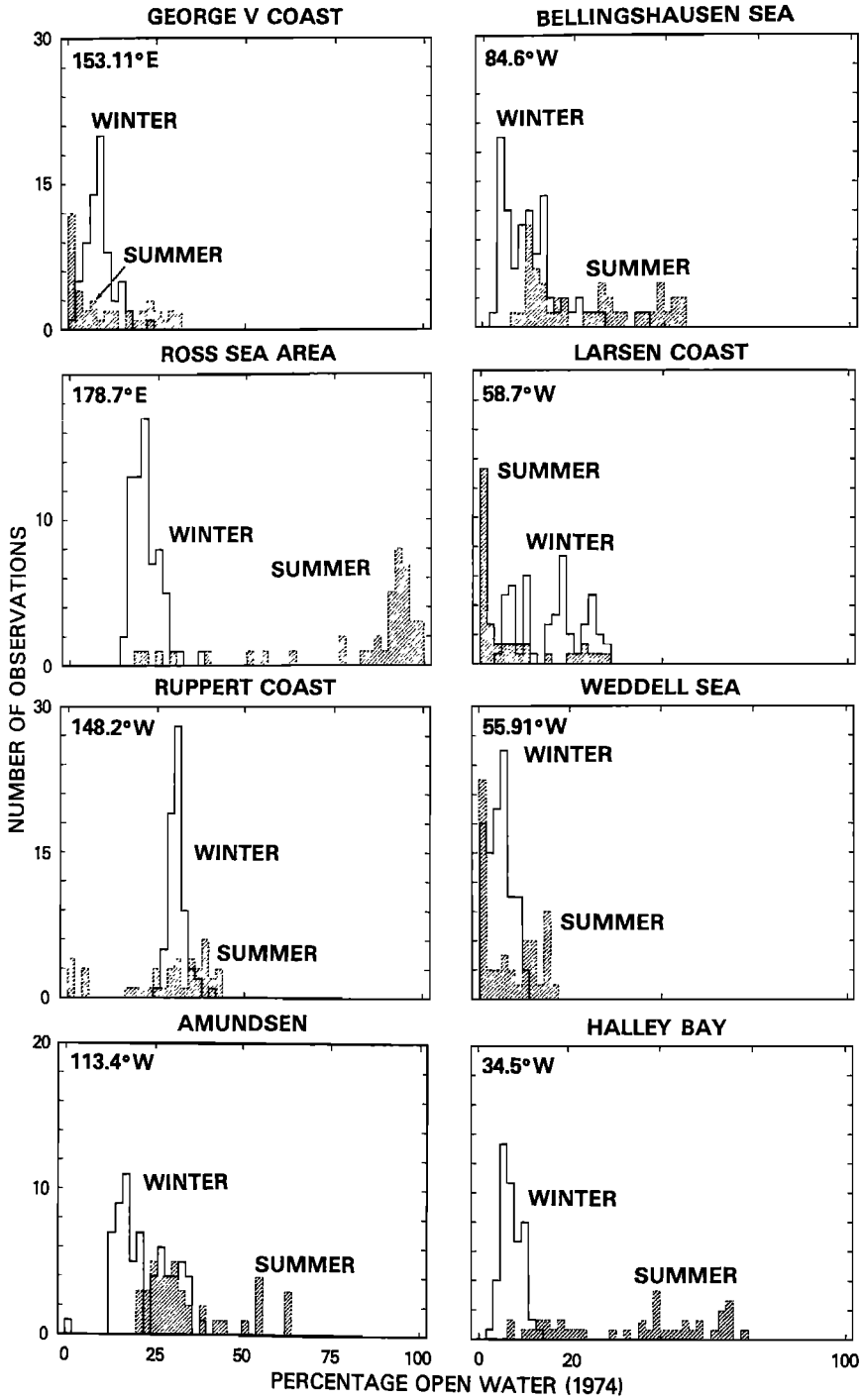

Fig. 25. Frequency distributions of the ratio of open water area to total area in each of the study regions from 153.1°E to 34.5°W.

assuming the newly formed ice has a salinity of 10.0, after Schumacher et al. [1983] and Cavalieri and Martin [this volume]. Also, Wakatsuchi and Ono [1983] report salt rejection values of 1.1 to 3.8 g cm^{-2} per meter of ice for ice growth rates ranging from 0.06 to 0.13 m/d), T is the duration in days of the winter period, (taken from day 76 through day 315, a total of 240 days), A is the observed ratio of open water to total surface area of

TABLE 2. Salinization of Water Volume Within Each Region Due to Sea Ice Formation with Open Water Fraction

Study Area	Midpoint Lat.	Midpoint Long.	Total Area A_T (km^2)	Open Water Ratio[a] A_W/A_T (%)	σ_A	Salinization[b] (‰) low	Salinization[b] (‰) high
Riiser-Larsen	69.0°S	34.3°E	27,260	0.201	0.04	0.233	0.396
Syowa	68.2°	41.3°E	18,740	0.134	0.06	0.155	0.264
Amery	68.2°	71.9°E	70,210	0.194	0.04	0.225	0.382
Prydz	67.3°	80.0°E	28,860	0.269	0.08	0.312	0.530
Shackleton	65.0°	99.4°E	47,580	0.281	0.06	0.325	0.553
Casey	66.0°	108.4°E	42,390	0.175	0.04	0.203	0.345
Sabrina	66.4°	116.9°E	36,010	0.121	0.05	0.140	0.238
Adélie	67.0°	147.5°E	47,390	0.254	0.06	0.294	0.500
George V	67.9°	153.1°E	53,250	0.098	0.03	0.114	0.193
Ross	77.5°	178.7°E	121,000	0.223	0.04	0.258	0.439
Ruppert	76.0°	148.2°W	40,120	0.319	0.02	0.369	0.628
Amundsen	72.9°	113.4°W	117,600	0.229	0.12	0.265	0.451
Bellingshausen	71.8°	84.6°W	197,100	0.147	0.06	0.170	0.289
Larsen	67.3°	58.7°W	119,300	0.203	0.12	0.235	0.400
Weddell	73.1°	55.9°W	283,800	0.066	0.04	0.076	0.130
Halley	76.7°	34.5°W	98,900	0.103	0.04	0.119	0.203
Average				0.189	0.06	0.218	0.371

[a]Ratio of winter-average open water area to total ocean area.
[b]From equation 3, with the values for R_i = 0.10 m/d, and h, s, and T given in the text, then $\Delta S = 1.158\ A_W/A_T$. The range of salinization values corresponds to R_i ranging from low, 0.10 m/d, to high, 0.17 m/d.

each study region (the value given in Table 2 represents the average ratio $\langle A_W \rangle / A_T$ for the 240-day winter period), R_i is the rate of ice formation in meters per day within the open water area (two values, 0.10 and 0.17 m/d, are used for the Table 2 determinations to represent the range of estimates),and h is the water column thickness for the study regions in meters (an average shelf depth of 518 m is used after Carmack [1977]).

Table 2 gives the ΔS values calculated for each of the 16 study regions. The average percentage of observed open water is 19% which gives a significant salinity enhancement of 0.220 to 0.374. Carmack [1977] shows that the largest volume of modified deep water within the shelf water column has a salinity of 34.4. If modified deep water is the initial ingredient of the cold (near freezing point) shelf water, an increase of 0.2 would in 1 year boost its salinity over 34.6, which is considered to be the minimum salinity required for formation of Antarctic Bottom Water.

Comparison of the calculated ΔS values with the measured salinity of near-freezing point shelf water versus longitude (Figure 5 of Gordon [1974]) shows that both values are high along the coast of East Antarctica. In the Weddell region, the calculated ΔS values are relatively low, yet the measured shelf-water salinity is high; thus other factors must also be important in determining shelf-water salinity. Equation (2) is, of course, a gross simplification and does not take into account redistribution of salt by circulation, variations in the value of the water column thickness, or the salinity of the initial water type. Nevertheless, ice generation within the 19% open water area on the shelf appears to be a major factor in raising the density of shelf water.

Discussion

Analysis of the microwave observations provides new information on the extent and variability of the open water in the Antarctic coastal regions. The temporal variability of the open water is observed to be large on daily to seasonal time scales. Spatial variability of the open water is also observed to be large on scales ranging upward from the 30-km resolution of the microwave sensor. Although 3-day averages are found to be adequate to resolve most of the major changes in open water described here as polynya events, the daily averages show more temporal detail and larger fluctuations between minima and maxima. On

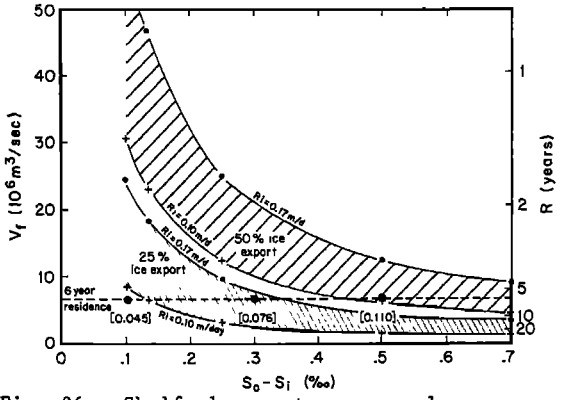

Fig. 26. Shelf-slope water mass volume exchange rate, V_F (10^6 m^3/sec), as a function of the salinity difference between the inflow (S_i) and outflow (S_o) water (see Figure 1), and the percentage of sea ice which forms on the shelf but is exported and melts seaward of the shelf (25 and 50% exported). The shelf water residence time in years is shown at the right. The calculations are carried out for R_i of 0.10 and 0.17 m/d (see text). The values in brackets along the 6-year residence line refer to the required R_i value, with sea ice export of 50%, which would yield that residence time.

monthly time scales, the polynya events are not resolved and are only evident as reduced average sea ice concentrations in the monthly average maps. The openings and closings of individual leads and polynyas are not resolved either in time or space, but the time-average maps represent the average open water during each period of observation.

While one or more 30 km x 30 km pixels often indicate 100% ice cover, the average concentration in most pixels is usually less than 100%. On spatial scales of the 16 study areas, the temporal variations in open water area occur above a significant background of open water. The persistent open water accounts for most of the winter-season average open water, which ranges from 7% to 32% in the various study areas. The results are considered to be representative of the shelf regions around Antarctica, because the study areas represent both regions with consolidated ice packs during winter and regions with significantly reduced ice concentrations or polynya events, as can be noted from the calculated open water values and a visual comparison of the ice concentrations along the coast in Plate 1.

The existence of substantial areas of open water in the Antarctic nearshore sea ice zone during winter has several important consequences. The flux of sensible and latent heat to the atmosphere is much greater from the open water areas than through a consolidated ice pack. Consequently, the growth of new ice in the open water areas is much greater than the growth at the underside of the ice in ice-covered areas. Also, the growth of new ice and nilas, followed by growth of thin young ice, enhances the total seasonal sea ice cover and the amount of salt rejected during the growth season. Overall, more ice is formed in the areas of reduced ice concentration in the coastal zone, the atmosphere is warmed more than it would be over a consolidated ice pack, and the salt rejected during freezing significantly increases the salinity and density of the water in the coastal regions.

The maintenance of open water over a given area of the ocean under freezing conditions requires an export of ice to balance the area covered by new ice. Also, the average shelf-water salinity is a result of the balance between salt rejection during ice growth and the introduction of fresher water from sea ice melt in summer, glacial run-off, excess precipitation over evaporation, and the exchange of water over the continental slope. The fraction of ice exported and the exchange of water between the shelf and deep ocean are major factors in determining the average salinity of the shelf waters, in addition to the amount of ice formed.

What is the contribution to the total sea ice cover of the southern ocean from ice formation within offshore open water? Ice formation rates of 0.10 to 0.17 m/d over a 240-day winter period would produce 24 to 41 meters of ice. Using 19% as a typical open water value for the shelf region (Table 2), ice production would then amount to 4.6 to 7.8 m if spread over the entire shelf. Those effective production rates would be about 15% lower if open water on the shelf were computed from an area-weighted average ratio. Sea ice production by bottom accretion in the other 81% of the area represents additional total ice volume. Thin ice (<0.30 m) grows much faster than thick ice, but not as fast as the initial ice growth in open water. If the spring sea ice cover of the shelf region ranges between 1.5 and 2.5 m [Jacobs et al., this volume], some ice must thicken by bottom accretion while other ice is exported to the north. Spread uniformly over the entire circumpolar belt of seasonal ice cover (about 20 x 10^6 km^2), ice formation in the offshore leads and polynyas would amount to 0.4 to 0.6 m, or approximately 50% of the mean ice thickness [Clarke and Ackley, 1984]. However, the ice formed at high-growth rates in the open water is redistributed in a complex manner as the ice pack diverges to maintain reduced ice concentrations. Although the open water adjacent to Antarctica is clearly a region of significant ice production compared to the total mass of the Antarctica seasonal ice cover, the actual distribution of the ice is determined by the ice drift after formation in the open water areas.

Salinization of the shelf water column by

ice production within the offshore leads and polynyas increases the likelihood of shelf water attaining density values sufficient to result in deep-reaching convective plumes over the continental slope [Killworth, 1983]. The total salt rejection associated with 4.6 to 7.8 m of sea ice over the 2.473 x 10^6 km^2 of shelf area [Carmack, 1977] is 2.8 to 4.8 x 10^{17} g/yr. A steady state shelf water salinity is maintained by the inflow of lower salinity water, but not all rejected salt needs to be balanced by shelf-slope water mass exchange because some sea ice melts on the shelf. Sea ice that forms and melts on the shelf has no net effect on shelf water salinity, although it can cause partitioning of salt. In addition, some of the salt is used to mix with the incoming fresh water due to excess precipitation over evaporation and glacial melt. Jacobs et al. [this volume] suggest a net fresh water input of 51 cm/yr to each cm^2 of shelf area. Conversion of this fresh water into average shelf water salinity (taken as 34.5) requires 0.43 x 10^{17} g/yr of salt.

The shelf-slope water volume exchange rate (V_f, Figure 1), required to balance net sea ice salt rejection by ice exported from the shelf depends on the difference between the inflow salinity (S_i) and outflow salinity (S_o) across the shelf-slope boundary. Adjusting for freshwater input and using the value for S_o-S_i of 0.134 with a sea ice export fraction of 50%, as suggested by Jacobs et al. (this volume), leads to a shelf-slope exchange rate of 23 to 47 x 10^6 m^3/sec, corresponding to residence times from 1.8 to 0.9 years (Figure 26). A residence time of 6 years (Jacobs et al., this volume), would require an ice export fraction of only 25% and a S_o-S_i difference ranging from 0.13 to 0.35. While these larger salinity differences are possible (if we simply invoke the ΔS calculated by equation 3 and given in Table 1), the export fraction of 25% seems too small.

A large source of uncertainity among these parameters is the rate of sea ice formation (R_i). For low R_i values ($\cong$ 0.03 m/d) and 50% sea ice export fraction, sea ice production would only compensate for the fresh water introduction and V_f would be zero. If the 0.10 m/d R_i were valid for only the 90 days studied by Cavalieri and Martin [this volume] and R_i were zero for the rest of the 240-day winter period, then the average growth rate for the full period would be 0.038 m/d. With a 50% export fraction and S_o-S_i of 0.134, V_f would be 2.5 x 10^6 m/s and the residence time would be 16 years. Alternatively, using the same export fraction (50%) and S_o-S_i value (0.134), R_i would have to be 0.051 m/d in order to yield a 6-year residence time.

Despite uncertainties in R_i, sea ice export fraction, and other parameters affecting the shelf water salinity, it is obvious that offshore leads and polynyas play an important role in southern ocean sea ice generation and salinization of the shelf water. Regional differences in the observed open water areas are large, and interannual variability may also be high. Further studies of the distribution of open water along the Antarctic coastline and of other related variables are needed to improve our knowledge of the quantitative oceanographic effects of these features.

Acknowledgments. The authors thank Steve Schweinfurth and Nancy Aschenbach of Science Applications Research, and Richard Johnson of Computer Sciences Corporation for programing help. The efforts of H.J.Z. and J.C.C. in this project were supported by NASA's Oceanic Processes Program. Lamont-Doherty Geological Observatory contribution 3792. A.L.G. support was derived from NSF grant DPP 81-19863.

References

Bromwich, D. H., and D. D. Kurtz, Experiences of Scott's Northern Party, Evidence for a relationship between winter katabatic winds and the Terra Nova Bay polynya, Polar Rec., 21, 137-146, 1982.

Bromwich, D. H., and D. D. Kurtz, Katabatic wind forcing of the Terra Nova Bay polynya, J. Geophys. Res., 89, 3561-3572, 1984.

Carsey, F. D., Microwave observation of the Weddell Polynya, Mon. Weather Rev., 108, 2032-2044, 1980.

Carmack E. C., Water characteristics of the southern ocean south of the polar front, A Voyage of Discovery, George Deacon 70th Anniversary Volume, edited by M. Azd, pp. 15-37, Pergamon Press, New York, 1977.

Cavalieri, D. J., and S. Martin, A passive microwave study of polynyas along the Antarctic Wilkes Land Coast, this volume.

Cavalieri, D. J., and C. L. Parkinson, Large-scale variations in observed Antarctic sea ice extent and associated atmospheric circulation, Mon. Weather Rev., 109, 2323-2336, 1981.

Clarke, D. B., and S. F. Ackley, Sea ice structure and biological activity in the Antarctic Marginal Ice Zone, J. Geophys. Res., 89, 2087-2095, 1984.

Comiso, J. C., Sea ice effective microwave emissivities inferred from microwave and infrared observations, J. Geophys. Res., 88, 7686-7704, 1983.

Comiso, J. C., and H. J. Zwally, Antarctic sea ice concentrations inferred from Nimbus 5 ESMR and Landsat imagery, J. Geophys Res., 87, 836-844, 1982.

Comiso, J. C., and H. J. Zwally, Concentration gradients and growth/decay characteristics of the seasonal sea ice cover, J. Geophys. Res., 89, 8081-8103, 1984.

Comiso, J. C., S. F. Ackley, and A. L. Gordon,

Antarctic sea ice microwave signatures and their correlation with in situ ice observations, J. Geophys. Res., 89, 662-672, 1984.

Dey, B., Applications of satellite thermal infrared images for monitoring North Water during the periods of polar darkness, Mon. Weather Rev., 93, 425-438, 1980.

Foster, T. D., and Carmack E. C., Frontal Zone mixing and Antarctic Bottom Water formation in the Southern Weddell Sea, Deep Sea Res., 23, 301-317, 1976.

Gloersen, P., T. T. Wilheit, T. C. Chang, W. Nordberg, and W. J. Campbell, Microwave maps of the polar ice of the earth, Bull. Amer. Meteorol. Soc., 55, 1442-1448, 1974.

Gordon, A. L., Varieties and variability of Antarctic Bottom Water, in Processees de Formation des Eaux Oceaniques Prefondes, Colloq. Int. CNRS, no. 215, pp. 33-47, Centre National de la Recherche Scientifique, Paris, 1974.

Gordon, A. L., Seasonality of southern ocean sea ice, J. Geophys. Res., 86, 4193-4197, 1981.

Gordon, A. L., Weddell deep water variability, J. Mar. Res., 40, 199-217, 1982.

Gordon, A. L., and B. A. Huber, Thermohaline stratification below the southern ocean sea ice, J. Geophys. Res., 89, 641-648, 1984.

Hibler, W., and S. F. Ackley, Numerical simulations of the Weddell Sea pack ice, J. Geophys. Res., 88, 2873-2887, 1983.

Jacobs, S., R. Fairbanks, and Y. Horibe, Origin and evolution of water masses near the Antarctic continental margin: evidence from $H_2{}^{18}O/H_2{}^{16}O$ ratios in sea water, this volume.

Killworth, P. D., On "chimney" formations in the ocean, J. Phys. Oceanogr., 9, 531-554, 1979.

Killworth, P. D., Deep convection in the world oceans, Rev. Geophys. Space Phys., 21, 1-26, 1983.

Kurtz, D. D., and D. H. Bromwich, Satellite observed behavior of the Terra Nova Bay polynya, J. Geophys. Res., 88, 9717-9722, 1983.

Martinson, D. G., P. D. Kilworth, and A. L. Gordon, A convective model for the Weddell Polynya, J. Phys. Oceanogr., 11, 406-488, 1981.

Maykut, G. A., Energy exchange over young sea ice in the central Arctic, J. Geophys. Res., 88, 3646-3657,1978.

Parish, T. R., The katabatic winds of Cape Denison and Port Martin, Polar Rec., 20, 525-532, 1981.

Parish, T. R., Surface airflow over east Antarctica, Mon. Weather Rev., 110, 84-90, 1982.

Parish, T. R., The influence of the Antarctic Peninsula on the wind field over the western Weddell Sea, J. Geophys. Res., 88, 2684-2692, 1983.

Parkinson, C. L., On the formation of the Weddell polynya, J. Phys. Oceangr., 13, 501-511, 1983.

Parkinson, C. L., and D. J. Cavalieri, Sea ice variations in the southern ocean, 1973-1975, Ann. Glaciol., 3, 249-254, 1982.

Priestley, R. E., General diary, 1 January 1912-February 1913, Doc. MS298/6/2, Scott Polar Research Institute, Cambridge, England, 1913.

Schumacher, J. D., K. Aagaard, C. H. Pease, and R. B. Tripp, Effects of a shelf polynya on flow and water properties in the northern Bering Sea, J. Geophys. Res., 88, 2723-2732, 1983.

Wakatshuchi, M., and N. Ono, Measurements of salinity and volume of brine excluded from growing sea ice, J. Geophys. Res., 88, 2943-2951, 1983.

Zwally, H. J., and P. Gloersen, Passive microwave images of the polar regions and research applications, Polar Rec., 18, 431-450, 1977.

Zwally, H. J., J. C. Comiso, C. L. Parkinson, W. Campbell, F. Carsey, and P. Gloersen, Antarctic sea ice satellite observations: 1973-1976, NASA Spec. Publ. SP459, 1983.

(Received July 9, 1984;
accepted December 26, 1984.)